The Plant Cell, Vol. 29: 2552–2569, October 2017, www.plantcell.org © 2017 ASPB.

ABA-Induced Stomatal Closure Involves ALMT4, a Phosphorylation-Dependent Vacuolar Anion Channel of Arabidopsis[OPEN]

Cornelia Eisenach,[a,1] Ulrike Baetz,[a] Nicola V. Huck,[b] Jingbo Zhang,[a,2] Alexis De Angeli,[c] Gerold J.M. Beckers,[b] and Enrico Martinoia[a]

[a] Department of Plant and Microbial Biology, University of Zurich, CH-8008 Zurich, Switzerland
[b] Department of Plant Physiology, Aachen Biology and Biotechnology, RWTH Aachen University, Aachen 52056, Germany
[c] Institute for Integrative Biology of the Cell (I2BC), CEA, CNRS, Université Paris-Sud, Université Paris-Saclay, 91198 Gif-sur-Yvette cedex, France

ORCID IDs: 0000-0003-4237-2278 (C.E.); 0000-0003-3072-7932 (A.D.A.); 0000-0002-5661-1666 (G.J.M.B.); 0000-0001-8943-7089 (E.M.)

Stomatal pores are formed between a pair of guard cells and allow plant uptake of CO_2 and water evaporation. Their aperture depends on changes in osmolyte concentration of guard cell vacuoles, specifically of K^+ and Mal^{2-}. Efflux of Mal^{2-} from the vacuole is required for stomatal closure; however, it is not clear how the anion is released. Here, we report the identification of ALMT4 (ALUMINUM ACTIVATED MALATE TRANSPORTER4) as an *Arabidopsis thaliana* ion channel that can mediate Mal^{2-} release from the vacuole and is required for stomatal closure in response to abscisic acid (ABA). Knockout mutants showed impaired stomatal closure in response to the drought stress hormone ABA and increased whole-plant wilting in response to drought and ABA. Electrophysiological data show that ALMT4 can mediate Mal^{2-} efflux and that the channel activity is dependent on a phosphorylatable C-terminal serine. Dephosphomimetic mutants of ALMT4 S382 showed increased channel activity and Mal^{2-} efflux. Reconstituting the active channel in *almt4* mutants impaired growth and stomatal opening. Phosphomimetic mutants were electrically inactive and phenocopied the *almt4* mutants. Surprisingly, S382 can be phosphorylated by mitogen-activated protein kinases in vitro. In brief, ALMT4 likely mediates Mal^{2-} efflux during ABA-induced stomatal closure and its activity depends on phosphorylation.

INTRODUCTION

Plants are in constant interaction with their environment. They take up carbon dioxide from the atmosphere for photosynthesis and release oxygen and water vapor in return. This exchange is essential for human life on earth, not only for the oxygen we breathe but also for the biomass produced through photosynthesis, its role in food production, as well as for the global water cycle. Plant gas exchange with the environment is facilitated through stomata, pores formed between a pair of guard cells. Guard cells swell to open the stomata and shrink to close these pores. Swelling and shrinkage depends on cell turgor, which is largely controlled by fluxes of osmotically active solutes into and out of the guard cell vacuole.

Ion channels and transporters at the plasma membrane and the vacuolar membrane (tonoplast) regulate fluxes of these ions during stomatal movement. Over the past four decades a wealth of information has been gathered regarding solute fluxes across the guard cell plasma membrane. However, in part due to the technical challenge of accessing an intracellular organelle for electrophysiological measurements, our knowledge of the transport processes across the vacuolar membrane during stomatal movement is still limited, especially regarding anion transport (Eisenach and De Angeli, 2017).

Vacuolar proton pumps acidify the vacuolar lumen and generate a proton gradient. The concomitant separation of charge establishes an electric potential gradient across the vacuolar membrane, i.e., the vacuolar membrane potential. The membrane potential reported in the literature is generally between 0 and −30 mV (Eisenach and De Angeli, 2017). In *Arabidopsis thaliana*, NHX-type transporters exploit the proton gradient to take up K^+ into the vacuole in exchange for protons (Andrés et al., 2014). During stomatal opening, guard cell K^+ content increases by nearly one order of magnitude, and 90% of this K^+ is stored in the vacuole (Roelfsema and Hedrich, 2005). Movement of only K^+ across the tonoplast would cause dramatic changes in membrane potential. Accordingly, K^+ is charge-balanced by counter ions, such as Cl^-, NO_3^-, and Mal^{2-}, which also act as osmotica (Roelfsema and Hedrich, 2005). Control of the vacuolar membrane potential is important since the activity of several ion channels depends on membrane voltage.

Mal^{2-} is the deprotonated form of malic acid, and the term malate refers to all protonation states of this dicarboxylic acid. With a pK_a of 5.2 for $Mal^{2-}/MalH^-$, Mal^{2-} is the dominant form in the cytosol and predominant in vacuoles of Arabidopsis guard cells (~80% Mal^{2-} at vacuolar pH 5.8). Early research highlighting

[1] Address correspondence to cornelia.eisenach@botinst.uzh.ch.
[2] Current address: Division of Biological Sciences, Section of Cell and Developmental Biology, University of California, San Diego, La Jolla, CA 92093.
The author responsible for distribution of materials integral to the findings presented in this article in accordance with the policy described in the Instructions for Authors (www.plantcell.org) is: Cornelia Eisenach (cornelia.eisenach@botinst.uzh.ch).
[OPEN]Articles can be viewed without a subscription.
www.plantcell.org/cgi/doi/10.1105/tpc.17.00452

the importance of Mal^{2-} as counter ion over inorganic ions such as Cl^- was performed in *Vicia faba* (Van Kirk and Raschke, 1978) and *Commelina communis* (MacRobbie and Lettau, 1980). In Arabidopsis, the guard cell malate concentration increases 2- to 3-fold during stomatal opening (Ding et al., 2014; Takahashi et al., 2015). The higher guard cell malate content of some Arabidopsis ecotypes corresponds with higher stomatal aperture and reduced stomatal closure (Monda et al. 2011, 2016; Takahashi et al., 2015) and the higher stomatal conductance in the anion channel knockout mutant *almt12* corresponds with higher accumulation of malate and other organic acids (Medeiros et al., 2016). Knockout mutants of ABCB14, which transports malate into guard cells, have altered stomatal response to CO_2 (Lee et al., 2008).

Given its weak acid properties, Mal^{2-} not only acts as an osmoticum, but its free cytoplasmic concentration should also influence cytoplasmic pH. Mal^{2-} might therefore have a role in regulating guard cell cytosolic pH, which is known to affect guard cell ion channels (for example, Gobert et al., 2007). Recently, it was shown that Mal^{2-} can also function as a signaling molecule at low cytosolic concentrations; Mal^{2-} activates the vacuolar Cl^- inward rectifying channel ALMT9 and causes enhanced Cl^- uptake during stomatal opening (De Angeli et al., 2013; Baetz et al., 2016).

In C_3 plants, stomata open in response to light during the day to allow for CO_2 uptake and its light-dependent photosynthetic assimilation. When the plant faces drought, however, stomata close in the light. Drought is signaled to the guard cells via the phytohormone abscisic acid (ABA), which causes rapid stomatal closure (Roelfsema and Hedrich, 2005). This response is crucial to prevent wilting and ensure plant survival. While we know how efflux of K^+ from the vacuole is achieved during stomatal closure in Arabidopsis (Gobert et al., 2007), our information on vacuolar anion efflux in general is sparse. Specifically, we do not know how Mal^{2-} efflux during stomatal closure is achieved. The anion H^+-antiporters CLCc and CLCa are important for uptake of Cl^- and NO_3^- during stomatal opening (Jossier et al., 2010; Wege et al., 2014), but knockout mutants also show impaired stomatal closure. For CLCa, this might be due to a stimulation of NO_3^- efflux activity in response to ABA (Wege et al., 2014).

Large and fast changes in ion concentration, such as those likely to occur during stomatal closure (MacRobbie, 1995b, 2006), are often mediated by ion channels (Hille, 2001; Chrispeels et al., 1999). Hence, it has been suggested that anion efflux from the vacuole could occur through vacuolar ALMT channels (Kollist et al., 2014). At the plasma membrane, ALMT12/ QUICK ANION CHANNEL1 (QUAC1) mediates anion current out of the cell and is required for stomatal closure (Meyer et al., 2010; Sasaki et al., 2010). ALMTs are a small gene family of anion channels. They were originally denoted as ALUMINUM ACTIVATED MALATE TRANSPORTERs (ALMTs) and identified as malate exporters conferring aluminum resistance. In Arabidopsis, this gene family comprises 13 members that cluster in four distinct phylogenetic clades (Dreyer et al., 2012). Clade II contains five members, *ALMT3*, *ALMT4*, *ALMT5*, *ALMT6*, and *ALMT9*, with ALMT9 and ALMT6 localized to the vacuole (Kovermann et al., 2007; Meyer et al., 2011). ALMT9 mediates voltage-dependent, inward Mal^{2-} currents, i.e., Mal^{2-} fluxes directed into the vacuole (Kovermann et al., 2007; Zhang et al., 2013; Bertl et al., 1992; Hafke et al., 2003). Surprisingly patch-clamp studies revealed that ALMT9 also acts as a guard cell, Mal^{2-}-activated Cl^- channel, and vacuolar Cl^- uptake through ALMT9 is required for stomatal opening (De Angeli et al., 2013). ALMT6 was identified as a potential vacuolar ion channel candidate to be involved in stomatal movement (Meyer et al., 2011). The channel is specifically expressed in guard cells of Arabidopsis, and patch-clamp analysis of guard cell vacuoles revealed that ALMT6 mediated Ca^{2+}- and voltage-dependent Mal^{2-} inward currents, mediating vacuolar Mal^{2-} uptake. Moreover, outward currents were detected at low vacuolar pH. Despite its guard cell-specific expression, no visible phenotype regarding stomatal aperture or whole-plant water use was found in *almt6* knockout plants. Therefore, the physiological role of ALMT6 in planta is still unclear.

Here, we report the identification of ALMT4 as a vacuolar anion channel in guard cells. Knockout mutants of *almt4* are impaired in stomatal movement in response to ABA, which suggests that this protein might be involved in solute loss from the vacuole. Indeed, ALMT4 is able to mediate Mal^{2-} efflux from the vacuole, and genetic and biochemical data strongly indicate that ALMT4's activity is controlled by phosphorylation.

RESULTS

Mutants of *ALMT4* Show Impaired Stomatal Closure and Increased Water Loss in Response to ABA, and Are More Susceptible to Drought

To investigate vacuolar ALMT channels potentially involved in stomatal movement, we focused on ALMT4, the clade II ALMT member most closely related to guard cell-specific ALMT6. We identified two knockout alleles (in the Col-0 and No-0 ecotypes) and corresponding wild-type-like outcrosses (referred to as the wild type). All plants were from the same seed batch and blind-analyzed.

Stomatal apertures were measured from epidermal peels of dark-adapted plants, after a 2-h light period and during a 0.5 and 2 h incubation with ABA (Figures 1A and B). Stomatal opening was not impaired in *almt4* mutants; however, stomatal closure in response to ABA was significantly slowed and incomplete (Figures 1A and B). After 0.5 h of ABA treatment, the Col-0 wild-type stomata had closed completely. When the difference between the dark-adapted and the light-adapted aperture was normalized to 100%, the wild-type aperture decreased in response to ABA by over 100%, indicating complete closure with respect to the dark state. When the same normalization was applied to *almt4*, the mutant closed by only ~40%. This difference was statistically significant, as was the difference in stomatal aperture after 2 h of ABA. In the No-0 background, differences between *almt4* knockout and wild type were more pronounced after 2 h of ABA treatment. Whereas the wild type displayed a stomatal aperture decreased by 95% compared with the initial dark value, the *almt4* mutant aperture decreased by only ~30%; this difference in degree of closure was statistically significant. The stomatal phenotype of both *almt4* mutant alleles is comparable to those of guard cell plasma membrane ion channel mutants involved in anion loss (*almt12/quac1*; Meyer et al., 2010) and K^+ loss (*gork*; Hosy et al., 2003).

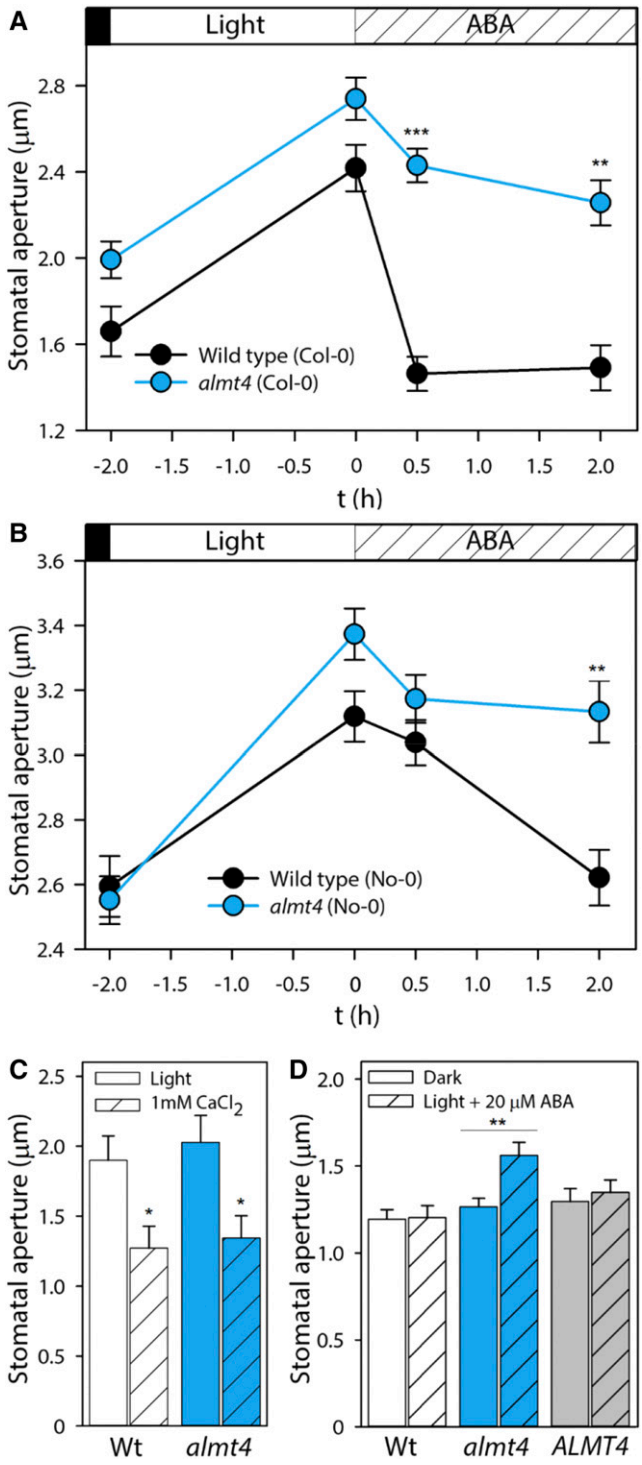

Figure 1. Responses of Stomatal Aperture to ABA and Ca^{2+}.

Stomatal aperture was measured on epidermal peels from the wild type, *almt4*, or an *ALMT4* complementation line.

(A) and **(B)** Aperture was measured from dark-adapted plants, after a 2-h incubation under white light and subsequent 0.5 and 2 h incubation with 20 µM ABA for the Col-0 **(A)** and the No-0 **(B)** allele. Significant differences were compared between lines within one time point.

(C) Aperture was measured after a 2-h incubation under white light (simple bars) and subsequent 2-h incubation with 1 mM $CaCl_2$ (shaded bars).

(D) Aperture was measured from dark-adapted plants (simple bars) and after 2-h incubation under white light and 20 µM ABA (shaded bars).

Data points are means of four different plants and for each plant, 60 stomata were analyzed (error bars denote the SE). Significance was analyzed by Student's *t* test and is indicated by asterisks: *P ≤ 0.05, **P ≤ 0.01, and ***P ≤ 0.001.

To confirm that impaired stomatal closure is indeed a function of the *ALMT4* gene product, we transformed *almt4* (Col-0) with a construct harboring the genomic *ALMT4* sequence fused to its native promoter (denoted: *ALMT4*). A complemented line was confirmed by RT-PCR (*ALMT4*-1; Supplemental Figure 1A) and investigated together with *almt4* mutant and the wild type in a second, independent experiment (Supplemental Figure 2). The impaired stomatal closure phenotype of *almt4* mutants was confirmed in this second experiment and was rescued in the complementation line. This result indicated that the *almt4* stomatal phenotype is associated with *ALMT4* function in guard cells.

A rise in the cytosolic free Ca^{2+} concentration is a signaling intermediate in ABA-induced stomatal closure (Roelfsema and Hedrich, 2010). However, Ca^{2+}-induced closure was not affected in the *almt4* mutant (Figure 1C). ABA not only induces closure but also inhibits stomatal opening. We tested whether ABA inhibition of stomatal opening was affected and, indeed, when simultaneously incubated with ABA, *almt4* mutant stomata opened in response to light, whereas stomata of the wild type and complementation line did not (Figure 1D).

The observed mutant stomatal phenotypes suggested a function for ALMT4 in whole-plant water balance. We therefore performed gas exchange experiments to analyze whole-plant ensemble stomatal behavior in response to dark and light stimuli (Supplemental Figures 3A and 3B). We found that there were no consistent differences in dark- or light-adapted transpiration rates between the wild type and *almt4* mutants of both ecotypes. Therefore, the altered stomatal behavior in *almt4* might be specific to ABA. To test whether the impaired ABA response in the mutant has an effect on the whole-plant level, we performed a water loss (Figures 2A and 2B) and a drought stress (Figure 2C) experiment. For the first experiment, petioles of rosettes leaves were incubated in ABA (Figure 2A) or a control solution (Figure 2B) for 1 h and then left to air dry. The fresh weight was monitored before and after drying, and the difference in fresh weight was interpreted as the percentage of water loss. To a large degree this water loss is due to stomatal transpiration, and we found that indeed *almt4* mutants of Col-0 and No-0 lost 55% and 50% of their water, respectively (Figure 2A). By contrast, corresponding wild types lost only 47% and 42% of water, respectively, and the mutant phenotype was rescued in the complementation line (46% water loss). When leaves were not pretreated with ABA, that is, stomata were not allowed to close before drying, no significant differences in water loss were detected between the mutant, wild type, and complementation line (Figure 2B).

During drought stress, whole plants synthesize ABA to aid stomatal closure and prevent wilting. To analyze if *almt4* mutants show an effect under physiological conditions, we performed

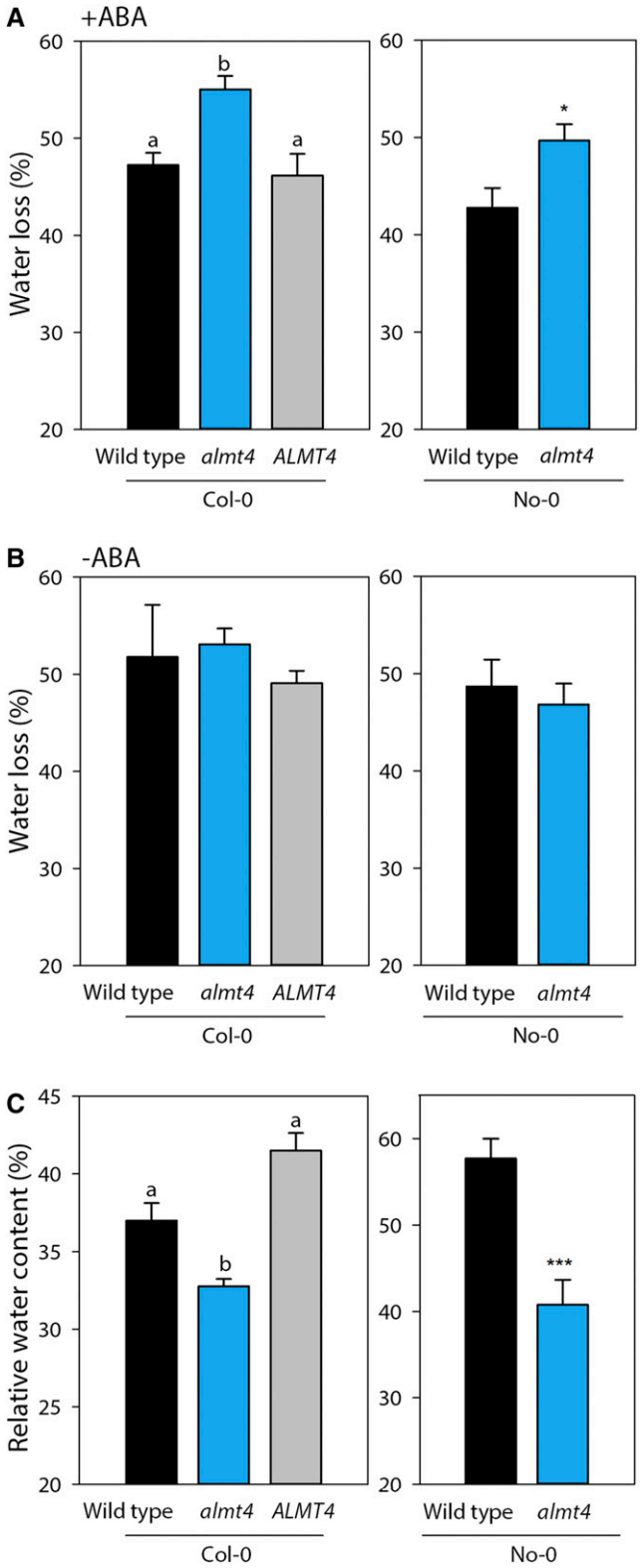

Figure 2. Whole-Plant Stomatal Phenotype in Response to ABA and Drought Stress.

a drought stress experiment. We withheld watering for 2 weeks, until plants showed obvious signs of wilting, and determined relative water content (RWC) of drought-stressed rosette leaves. After drought stress, *almt4* mutants had a significantly lower RWC (32 and 41% Col-0 and No-0, respectively) when compared with the wild type (37 and 58%, Col-0 and No-0, respectively) and the complementation line (42%; Figure 2C).

The observed phenotypes did not result from pleiotropic effects caused by differential expression of other members of the clade II *ALMT* family. Expression levels of all clade II *ALMT* mRNAs were not significantly different between the wild type and *almt4* (Supplemental Figure 1B).

ALMT4 Is Localized to the Vacuolar Membrane and Is Expressed in Leaf Mesophyll and Guard Cells

Next, we examined intracellular, organ, and tissue-specific localization of ALMT4. *ALMT4* was cloned from Arabidopsis rosette leaf cDNA, and transiently expressed in *Nicotiana benthamiana* with a C-terminal fusion to GFP. Fluorescence was observed intracellularly in intact epidermis cells. When we isolated protoplasts and lysed them using an osmotic shock treatment to release the central vacuole, GFP fluorescence was clearly visible at the vacuolar membrane (Figures 3A to 3D).

We investigated organ-specific expression by qRT-PCR analysis (Figure 4A). *ALMT4* was expressed throughout the plant at similar levels in roots, rosette leaves, cauline leaves, and stem. Expression was overall lower in seeds and seedlings and highest in siliques and flowers. The *almt4* mutant phenotypes suggested *ALMT4* expression in guard cells. To analyze tissue-specific expression, we fused a 1.8-kb promoter fragment of *ALMT4* to the *GUS* reporter gene ($ALMT4_{Pro}$:GUS). GUS reporter activity was found throughout the plant in cotyledons and leaves (Figures 3E and 3L to 3N), in the vasculature and cortex of the hypocotyl (Figures 3F to 3H), and in the root vasculature (Figure 3I). In leaves, GUS activity was high in the leaf vasculature (Figure 3J), the mesophyll (Figures 3E, 3M, and 3N), hydathodes (Figure 3K), and guard cells (Figures 3L and 3O). Furthermore, GUS reporter gene activity increased when rosettes were preincubated in ABA (Figure 3N). Usually, staining was observed in mesophyll and guard cells, but after ABA treatment, guard cell staining increased compared with mesophyll staining (Figure 3O).

In the absence of public expression data, further evidence for guard cell expression of *ALMT4* came from a study on RNA

(A) and **(B)** Water loss of air-dried rosette leaves of Col-0 and No-0 lines (n = 6). ABA (**[A]**; 20 μM in double-distilled water, final concentration of 0.2% ethanol) or a control solution (**[B]**; double-distilled water, final concentration of 0.2% ethanol) was fed to leaves via petioles for an hour in the light, and leaves were left to air-dry in the light for 7 h. Fresh weight was recorded before and after drying and water loss was calculated.

(C) RWC of rosette leaves from 10 individual, soil-grown plants per line after the plants had been exposed to drought stress.

Data are means ± SE and were analyzed either by ANOVA followed by multiple pairwise comparison or Student's t test. Significances by ANOVA are indicated by lettering with different letters denoting significant differences ($P \leq 0.05$) and significance for t test by asterisks (*$P \leq 0.05$, **$P \leq 0.01$, and ***$P \leq 0.001$).

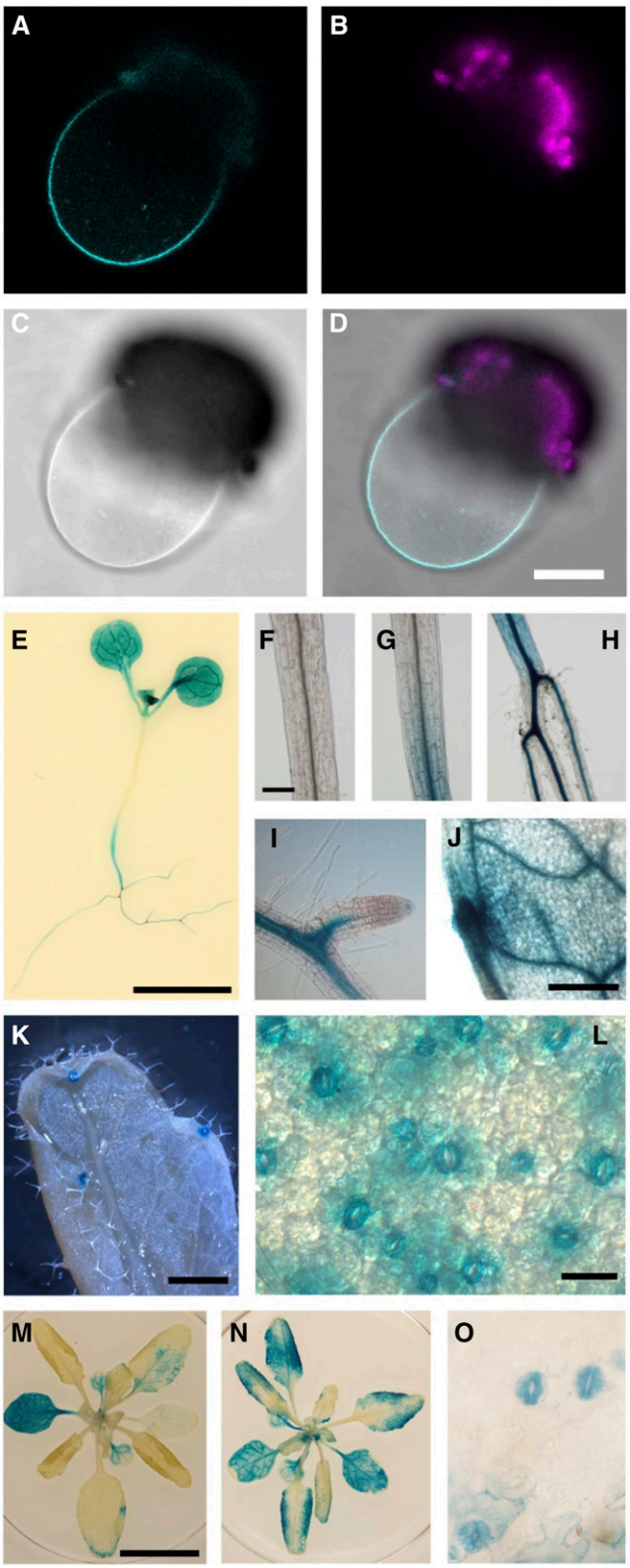

Figure 3. Localization and Expression of ALMT4.

(A) to **(D)** ALMT4-GFP transiently expressed in *N. benthamiana* localizes to the vacuolar membrane of a lysed protoplast (**[A]** to **[D]**). GFP fluorescence (cyan; **[A]**), chlorophyll fluorescence from protoplast debris (magenta; **[B]**), bright field **(C)**, and overlay **(D)**. Bar = 25 μm.

(E) to **(O)** An $ALMT4_{Pro}$:GUS construct causes reporter gene expression in seedlings (**[E]**; bar = 5 mm), specifically in the hypocotyl (**[F]**, shoot; **[G]**, shoot-hypocotyl transition; **[H]**, hypocotyl-root transition; bar = 200 μm), in the vasculature of roots (**[I]**; bar = 50 μm) and leaves (**[J]**; bar = 500 μm), and in hydathodes (**[K]**; bar = 1 mm), stomata and mesophyll cells (**[L]**; bar = 20 μm). Reporter gene expression in mature whole rosettes (**[M]**; bar = 1 cm) increased when rosettes were incubated in 20 μM ABA for 2 h at room temperature (**[N]**; scale as in **[M]**), and ABA caused expression in guard cells without concurrent mesophyll staining (**[O]**; scale as in **[L]**).

isolation from guard cells (Obulareddy et al., 2013). The released mRNA expression data for all *ALMT* members of clade II are visualized in Figure 4B. The data show that *ALMT4* is expressed at a level similar to *ALMT9* in guard cells and that the expression of *ALMT6* is about 10 times lower compared with *ALMT9*.

ALMT4 Macroscopic Currents Resemble Those of ALMT9 but Show Distinct Kinetics and Rectification

Taken together, the above data suggest a function for ALMT4 at the guard cell vacuolar membrane, necessary for stomatal closing. By contrast, ALMT9 functions at the guard cell vacuolar membrane but is necessary for stomatal opening, mediating Cl^- uptake into the vacuole (De Angeli et al., 2013). The opposite mutant phenotypes suggested a mechanism for ALMT4 opposite to that of ALMT9, i.e., that ALMT4 might carry anion currents in the opposite direction, from the vacuole to the cytoplasm. We used ALMT4-GFP expression in the vacuolar membrane of *N. benthamiana* to study the channel's electrophysiological characteristics by patch-clamp (Figure 5). We obtained excised outside-out patches and used symmetric Mal^{2-} conditions, with 100 mM Mal^{2-} in the pipette, representing the vacuolar side (Mal^{2-}_{vac}), and 100 mM Mal^{2-} in the bath, representing the cytoplasmic side (Mal^{2-}_{cyt}). To analyze the current-voltage (I-V) relationship, we applied a voltage clamp protocol as shown in Figure 5A. For comparison, we also measured background currents and currents through ALMT9 (Figures 5B and 5C). ALMT9 displayed typical inwardly directed Mal^{2-} currents that activated between 0 mV and −20 mV (Figures 5B and 5C), as has been reported previously (Kovermann et al., 2007; De Angeli et al., 2013; Zhang et al., 2013, 2014). Surprisingly, 30% of all patches obtained for ALMT4 displayed current with mean amplitudes smaller than 100 pA at −120 mV, i.e., they were indistinguishable from background currents. This finding suggested that the data were pools of two different populations. Indeed, a normality test of current distribution at −120 mV show that data were not normally distributed, and a histogram showed that the data cluster in two groups (Supplemental Figure 4). One group overlapped with the distribution of background current data and probably represents current from largely inactive ALMT4 channels. We therefore grouped all data with mean amplitudes that overlapped with background currents, i.e., below 100 pA at −120 mV, and excluded them from any further analysis. Active ALMT4 currents were inwardly directed and yielded a mean steady state amplitude of −282 pA ± 30 pA at −120 mV, about 4 times lower than that of

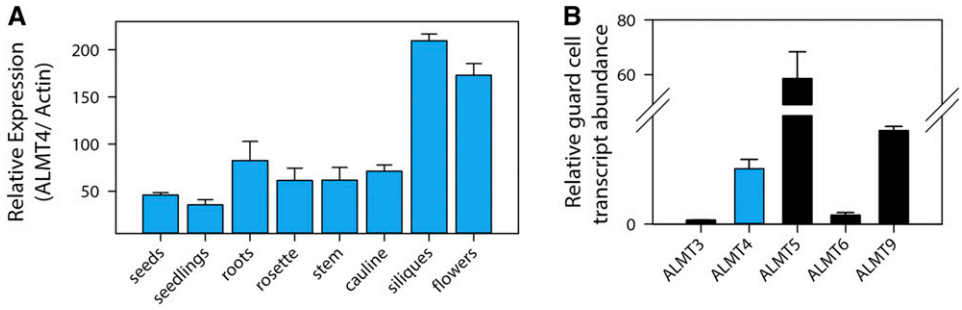

Figure 4. Expression of *ALMT4* throughout the Plant and in Guard Cells.

(A) *ALMT4* expression was quantified by qRT-PCR across a range of plant organs. Data are shown as mean ± SD ($n = 2$ independent experiments with five plants and three technical replicates each); *ACTIN2* served as a reference gene; expression was normalized to *ALMT4* mRNA levels in seeds.
(B) Abundance of clade II *ALMT* mRNAs in guard cells, relative to guard-cell-specific ALMT6. Data were taken from Obulareddy et al. (2013), and originally reported as fragments per kilobase of exon per million fragments mapped. Data are means ± SD from two samples.

ALMT9 (Figure 5C), despite similar GFP fluorescence at the tonoplast.

We tested whether ALMT4-mediated currents might be low because Mal^{2-} is not the preferred permeating substrate by substitution of the cytosolic side solution with buffers based on different anions (Figure 5E). Among the organic ions, ALMT4 was permeable to Mal^{2-} and fumarate (Fum^{2-}) but not to citrate (Cit^{3-}). Using reversal potential analysis, we found that ALMT4 was 1.8 times more permeable to Fum^{2-} compared with Mal^{2-}. Among the anions, ALMT4 was not permeable to Cl^-, NO_3^-, HPO_4^{2-}, and SO_4^{2-}, but we detected an activation of Cl^- current by 1 mM Mal^{2-}, similar to what was previously reported for ALMT9. Although Arabidopsis contains high fumarate levels compared with many other species (Chia et al., 2000; Araújo et al., 2011), a role for fumarate in Arabidopsis guard cell physiology is hardly documented in the literature. Although, like ALMT9, ALMT4 can transport Cl^- into the vacuole when activated by Mal^{2-}, the stomatal phenotypes are contrary to this notion, so that at least for guard cells, we exclude a role of ALMT4 in Cl^- uptake. Therefore, we concentrated on Mal^{2-} as a substrate in our electrophysiological experiments.

Besides differences in channel activity and macroscopic current amplitude, ALMT4 macroscopic current kinetics differed significantly from those of ALMT9. Activating and deactivating current kinetics reflect transition reactions between the open and the closed state of ion channels. They can be fitted by exponential functions to derive time constants (τ) that inform on the rates of the state transitions (Supplemental Figure 5; see Methods). While the time constant for current activation ($\tau_{Activation}$) at −120 mV was similar between both channels (Figure 5D, Table 1), the time constant for deactivation ($\tau_{Deactivation}$) of ALMT4 was about 4 times larger than that of ALMT9. This finding indicated that channel closing in response to a deactivating voltage took longer in ALMT4 channels. Furthermore, we examined the open channel rectification of ALMT9 and ALMT4 by determining the rectification rate (Figure 5D). The rectification rate is the ratio of activated channel steady state conductance at −120 mV ($G_{act-120}$) and open channel conductance at the deactivating tail voltage (+60 mV; $G_{tail+60}$; see Supplemental Figure 5). It denotes the preference of the permeation pathway for inward or outward rectification. We found that ALMT4 displayed a rectification rate significantly increased by more than 4-fold when compared with that of ALMT9 (Table 1, compared with Zhang et al., 2013). The large rectification rate of ALMT4, compared with ALMT9, indicates that its propensity to conduct inward ion fluxes is similar to its propensity to conduct outward current fluxes; thus, ALMT4 might be more prone to mediate Mal^{2-} outward currents.

ALMT4 Is Phosphorylated at S382 and Currents Are Activated by Dephosphomimetic Mutation

ALMT4 current generally displayed a low macroscopic steady state current amplitude and activity. ALMT12/QUAC1 also displayed a low basal activity (Meyer et al., 2010) but was markedly activated by OST1-mediated phosphorylation in response to ABA (Imes et al., 2013).

The ABA-related *almt4* phenotypes led us to test recombinant OST1 on ALMT4. We patched vacuoles expressing ALMT4 in experiments analogous to those shown in Figure 5. Once stable ALMT4 currents were recorded, we perfused the membrane patch with a bath solution containing recombinant OST1 together with ATP, constantly monitoring current activity. However, no changes in current activity or I-V relations could be detected upon application of the kinase (data not shown). ATP on its own had no effect on the current.

In the search for other putative phosphorylation sites, we mined the public PhosPhAt database (Heazlewood et al., 2008) and found a phosphoproteomic data set containing a phosphopeptide of ALMT4, showing phosphorylation at S382 [MEKL(p)SPGNVLK; Figure 6A]. S382 is located within the C-terminal moiety of the protein, which is predicted to be localized in the cytoplasm (Figure 6A). To test the significance of S382 phosphorylation for ALMT4 function, we generated ALMT4 S382E and ALMT4 S382A constructs, i.e., introduced phosphomimetic and dephosphomimetic mutations, respectively. Expression of both constructs at the tonoplast was confirmed by fluorescence microscopy before performing patch-clamp analysis as described above. We found a striking difference in Mal^{2-} currents and I-V relations between both constructs (Figures 6B and 6C). In all patches expressing ALMT4 S382E-GFP, we detected only background current activity

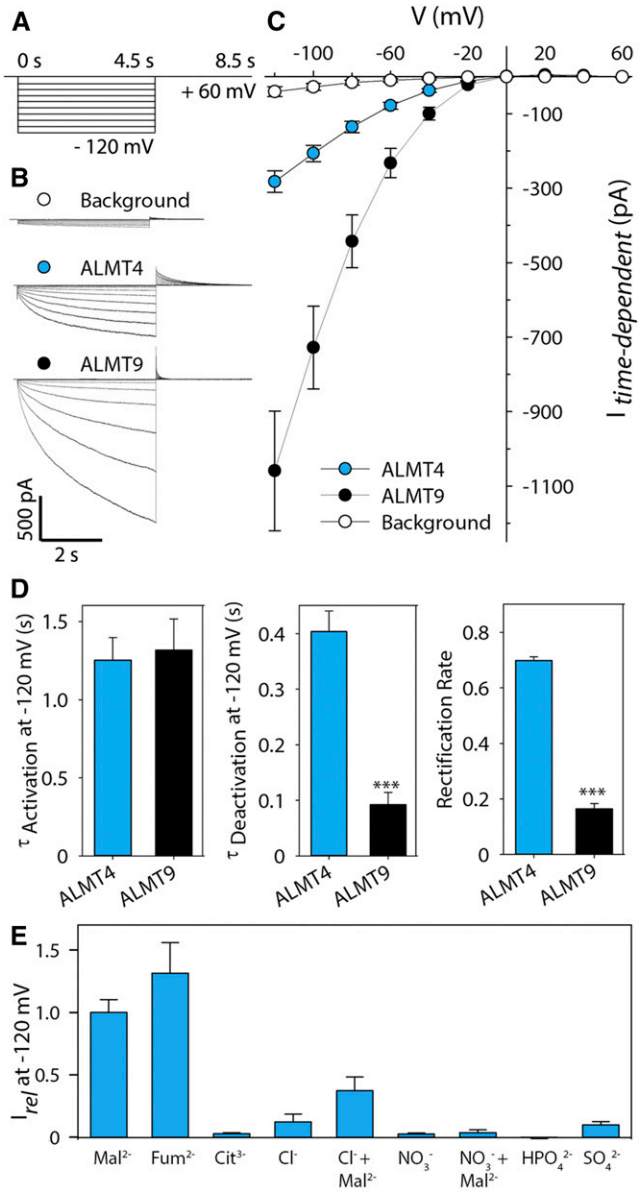

Figure 5. Comparison of ALMT4- and ALMT9-Mediated Currents.

(A) Schematic representation of the voltage protocol used. Activating currents were evoked by successive voltage pulses ranging from a holding voltage of +60 mV to −120 mV and recorded for 4.5 s, with successive voltage pulses increasing by 20 mV. Deactivating tail currents were recorded for 4 s by a subsequent step to holding voltage.

(B) Representative current traces of background current from untransformed vacuoles (top, white), ALMT4 (middle, blue), and ALMT9 (bottom, black).

(C) I-V curve of background (white circles, $n = 11$), ALMT4 (blue circles, $n = 11$), and ALMT9 (black circles, $n = 12$) time-dependent currents at steady state in symmetric Mal^{2-} conditions (100 mM Mal^{2-}_{vac}/100 mM Mal^{2-}_{cyt}). Currents were measured on excised outside-out patches of *N. benthamiana* vacuoles, either untransformed or confirmed to express ALMT9-GFP or ALMT4-GFP. Data points are means of current means at steady state. Error bars denote the SE.

(D) Time constants for activating (left) and deactivating (middle) time-dependent current at −120 mV and rectification rate (right). For analysis methods, see Supplemental Figure 5 and Methods. Data are means ± SE.

(E) Current means for different substrates relative to Mal^{2-} current at −120 mV ($n = 3$) ± SE. In case of Cl^- and NO_3^-, 1 mM Mal^{2-} was added to investigate potential current activation.

(compared with Figures 6C and 5C). ALMT4 S382E yielded a mean current amplitude of −30 pA ± 12 pA at −120 mV (Figure 6C). However, patches expressing ALMT4 S382A-GFP yielded a mean current amplitude of −502 pA ± 73 pA at −120 mV, nearly double that of the wild-type channel (compared with Figures 6C and 5C). Furthermore, the percentage of patches showing background current activity was decreased (Figure 6D). In summary, these data show that mutation of ALMT4 S382 to glutamate causes background current amplitudes, suggesting that phosphorylation is required and sufficient for channel deactivation. Mutation to alanine causes an increase in channel activity as well as an increase in macroscopic Mal^{2-} current amplitude, suggesting that dephosphorylation is required for channel activation, but other factors might also contribute.

The *almt4* Mutants Transformed with Active ALMT4 S382A or Inactive ALMT4 S382E Display Distinct Growth and Stomatal Phenotypes

To investigate whether S382 of ALMT4 does play a role in vivo and whether phosphorylation at this residue might underpin the observed *almt4* stomatal phenotype, we transformed the *almt4* mutant (Col-0) with ALMT4 S382A and S382E constructs, termed *S382A* and *S382E*, respectively. Surprisingly, *S382A* lines showed a strongly reduced rosette area and fresh weight (Figures 7A and 7C). Evidently, expression of constitutively active ALMT4 causes severe growth defects. Epidermal peels of the transformants, *almt4* mutant, and the wild type were examined in an experiment akin to that shown in Figure 1. As found in the previous experiments, the *almt4* mutant stomata opened during a 2-h light treatment but showed delayed and incomplete closure upon treatment with 20 μM ABA (Figure 7B, compared with Figure 1A). Strikingly, *S382A* expressing the constitutively active channel displayed a marked impairment in stomatal opening, showing ~42 and 46% less opening than *almt4* and the wild type, respectively. However, stomata of *almt4* transformed with the constitutively inactive channel (*S382E*) displayed wild-type-like opening behavior (Figure 7B). Stomatal closure in *S382E* was comparable to *almt4*, with stomata closing by 40% (compared with the dark value) in both cases, whereas wild-type stomata closed by 96% (Figure 7B). Stomata of *S382A* closed by only 12%. Comparable results were obtained with lines from independent transformation events (Supplemental Figure 6).

These results show that mutating S382 has a dramatic effect on plant growth and stomatal movement and suggest that the S382A mutation prevents guard cell solute accumulation and efficient stomatal opening. This conclusion suggested that active ALMT4 might be involved in solute loss from the vacuole and be able to mediate Mal^{2-} efflux at the prevailing membrane potential.

Active ALMT4 S382A Mediates Mal^{2-} Outward Currents

To test whether ALMT4 S382A can mediate Mal^{2-} efflux from the vacuole, we devised a slow voltage-clamp protocol with

Table 1. Macroscopic Open Channel Currents (I_{tail0}) of Vacuolar Excised Outside-Out Patches Expressing ALMT9, ALMT4 S382A, and ALMT4 Wild Type Were Fitted by a Boltzman Function (Equation 3)

Parameter of Gating and Current Kinetics	ALMT9 (n = 7)	ALMT4 Wild Type (n = 8)	ALMT4 S382A (n = 8)
I_{tail0} max (pA)	121 ± 38[a]	142 ± 16[a]	256 ± 18[b]
$V_{1/2}$ (mV)	−90 ± 10[a]	−63 ± 4[b]	−67 ± 1[b]
z_g	0.7 ± 0.1	0.7 ± 0.02	0.7 ± 0.01
$\tau_{Activation}$	1.3 ± 0.2	1.3 ± 0.1	1.2 ± 0.4
$\tau_{Deactivation}$	0.1 ± 0.02[a]	0.4 ± 0.04[b]	0.4 ± 0.1[b]
R	0.2 ± 0.02[a]	0.7 ± 0.01[b]	0.8 ± 0.1[b]

From the fit, the maximal I_{tail0} (I_{tail0} max), the half-maximal activation voltage ($V_{1/2}$), and the gating charge (z_g) were derived. The time-dependent current proportion of activating currents and deactivating tail currents were fitted by standard exponential functions to derive activating ($\tau_{Activation}$) and deactivating ($\tau_{Deactivation}$) time constants. The rectification rates (R) were derived by dividing the steady state time-dependent conductance at the deactivating tail voltage of +60 mV by the conductance at the activating voltage of −120 mV. Data are averages ± SE. Significant differences were tested for each parameter by ANOVA followed by Holm-Sidak multiple comparison ($P \leq 0.001$) and are indicated by different letters.

longer-lasting voltage steps increasing by 10 mV, in order to resolve such a current (Figure 8A). Indeed, the I-V relation displayed positive outward currents at voltages positive of the reversal potential for Mal^{2-} ($E_{Rev}Mal^{2-}$ = 0 mV in symmetric ionic conditions; Figures 8B and 8C). The maximal steady state mean current amplitude of active ALMT4 S382A was 13 pA ± 4 pA at +20 mV. Within the same set of experiments, we also investigated ALMT9 and found only very small outward currents at positive voltages, with a mean steady state current amplitude of 2 pA ± 1 pA at +20 mV (Figures 8B and 8C). To examine the reason for the difference in ability to conduct outward current between ALMT4 S382A and ALMT9, we compared the relative open probabilities ($P_o rel$) of both channels (Supplemental Figure 5; see Methods). $P_o rel$ is proportional to I_{tail0} according to equation 2 (see Methods) and Boltzman analysis of I_{tail0} (Figure 8C, inset; equation 3; see Methods) indicated that, compared with ALMT9, ALMT4 S382A displayed a marked and statistically significant shift of the $V_{1/2}$ by 22 mV to more positive voltages (Table 1). ALMT4 S382A was not significantly different from wild-type ALMT4 in its gating characteristics, macroscopic current kinetics, and rectification ratio (Table 1). Considering that Mal^{2-} current typically activates between 0 mV and −20 mV in ALMT9 in symmetric Mal^{2-} conditions, the positive-going shift in $V_{1/2}$ explains why ALMT4 S382A is open at voltages positive of the reversal potential for Mal^{2-} (here, 0 mV) and able to mediate outward current along the electric gradient.

In planta, the Mal^{2-} concentration gradient is directed out of the vacuole, with lower cytosolic and higher vacuolar malate concentrations (Gerhardt and Heldt, 1984). We applied a 10-fold Mal^{2-} concentration gradient and observed a shift in outward current to more negative voltages, consistent with the concomitant shift in reversal potential (Figure 8D). Also, the current amplitude was diminished, with the highest outward current amplitude of active ALMT4 S382A at 5 pA ± 1 pA. This was also true for ALMT9, which nonetheless showed negligible outward current, consistent with the results displayed in Figure 8C. The decrease in current amplitude could reflect a sensitivity of the channel gate to the cytoplasmic Mal^{2-} concentration, to avoid Mal^{2-} efflux from the vacuole. However, it is not the case for ALMT4 S382A, since we did not observe a shift in $V_{1/2}$ between 10 and 100 mM Mal^{2-} (Supplemental Table 1). This lack of a shift shows that the channel is open to allow Mal^{2-} efflux at 10 mM $Mal^{2-}{}_{cyt}$. Furthermore, ALMT4 S382A displayed defined tail currents at outward current voltages (Figure 8D, inset; Supplemental Table 1, $I_{tail\ deact}$), confirming that the channel is open and able to mediate Mal^{2-} efflux from the vacuole at 10 mM $Mal^{2-}{}_{cyt}$. However, the time constant for activation was larger at 10 mM $Mal^{2-}{}_{cyt}$ (Supplemental Table 1, $\tau_{Activation}$), indicating that it takes longer for macroscopic currents to reach maximal outward amplitudes. This finding could explain the decrease in outward current amplitude at 10 mM $Mal^{2-}{}_{cyt}$, although other factors likely contribute to this phenomenon.

ALMT4 Is Phosphorylated by MAP Kinases in Vitro

The accumulated data suggest that ALMT4 is phosphorylated in vivo and that this phosphorylation causes inactivation of vacuolar Mal^{2-} fluxes. We asked which type of kinase might be responsible for this phosphorylation. Thus, we screened the amino acid sequence containing the phosphorylated S382 for motifs of canonical kinases implicated in abiotic stress signaling in guard cells, such as Ca^{2+}-dependent kinases or OST1, albeit to no avail. We noticed that S382 is followed by a proline, indicating that it might be the target of a proline-directed kinase.

Mitogen-activated protein kinases (MPKs) are proline-directed serine/threonine kinases. To test whether the S382-bearing C terminus of ALMT4 could indeed be phosphorylated by an MPK, we conducted a kinase assay. We GST-tagged the cytosolic C-terminal part of wild-type ALMT4 (GST-$ALMT4^{WT}$) and used site-directed mutagenesis to exchange S382 to Ala (GST-$ALMT4^{S382A}$). Along with GST-$ALMT4^{WT}$ and GST-$ALMT4^{S382A}$, we also prepared recombinant MPK4 and MPK6 to test whether these kinases can phosphorylate S382 of ALMT4 because the role of these kinases in ABA-mediated stomatal closure had been investigated previously (Hettenhausen et al., 2012; Xing et al., 2008; Montillet et al., 2013). We performed a recently established kinase assay that allows the detection of in vitro-phosphorylated MPK substrates by immunoblotting analyses (Leissing et al., 2016). As shown in Figure 9, activated recombinant MPK4 and

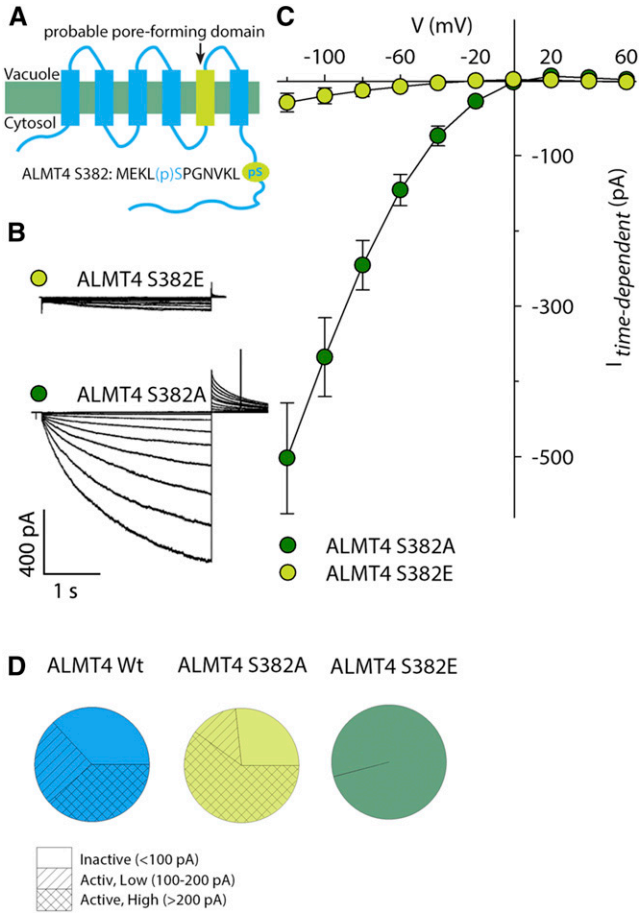

Figure 6. Identification of a Phosphorylation Site in the ALMT4 C Terminus and Comparison of Site-Directed Mutant Currents.

(A) Schematic representation of the presumed ALMT4 topology showing the probable pore-forming domain as determined by Zhang et al. (2013) and the approximate position of a phosphopeptide retrieved from the PhosPhAt database.

(B) Representative current traces of ALMT4 S382E (light green) and ALMT4 S382A (dark green).

(C) I-V curve of ALMT4 S382A (dark green circles, $n = 11$) and ALMT4 S382E (light green circles, $n = 9$) time-dependent currents at steady state in symmetric Mal^{2-} conditions (100 mM $Mal^{2-}{}_{vac}$/100 mM $Mal^{2-}{}_{cyt}$). Currents were measured on excised outside-out patches of *N. benthamiana* vacuoles confirmed to express ALMT4 S382E-GFP and ALMT4 S382A-GFP and were evoked by a voltage protocol as described in Figure 5.

(D) Distribution of wild-type and mutant ALMT4 current amplitudes at −120 mV in ALMT4 wild type (blue), ALMT4 S382A (light green), and ALMT4 S382E (dark green). Current amplitudes below 100 pA were classified as inactive (empty), between 100 and 200 pA as low amplitude active (dashed), and above 200 pA as high amplitude active (crossed).

MPK6 strongly phosphorylated GST-ALMT4^{WT}. By contrast, when S382 was mutated to Ala (GST-ALMT4^{S382A}), neither of the two MPKs was able to phosphorylate the protein (Figure 9). These results indicate that MPK4 and MPK6 can phosphorylate the ALMT4 C terminus at position S382 in vitro.

DISCUSSION

Stomatal closure requires retrieval of solutes from the guard cell vacuole, including Mal^{2-}, which can act as an osmoticum and charge-balances K^+. However, to date it has been unclear how Mal^{2-} is released from the vacuole during stomatal closure and the identity of the transport proteins has been obscure.

Here, we provide genetic and physiological evidence that ALMT4, a clade II member of Arabidopsis ALMT channels, mediates vacuolar Mal^{2-} efflux during drought stress-induced stomatal closure and that the channel is regulated by phosphorylation. Three key findings lead us to this conclusion. First, loss of function of *ALMT4* causes normal stomatal opening but delayed and incomplete stomatal closure in response to ABA, as well as increased water loss during drought and ABA treatment. Second, electrophysiological measurements show that ALMT4 is a voltage-dependent Mal^{2-} channel with distinct gating properties and rectification that allow Mal^{2-} efflux through it. Third, ALMT4 was deactivated by a S382E phosphomimetic mutation in patch-clamp studies and S382 could be phosphorylated by MPKs in vitro. In planta, the inactive channel (*S382E*) mimicked the *almt4* mutant, whereas the constitutively active channel (*S382A*) showed impaired stomatal opening and stunted growth.

Function of ALMT4 in the Plant

Our electrophysiological data show that ALMT4 is permeable to Mal^{2-}, Fum^{2-}, and Cl^- when activated by cytosolic Mal^{2-}. Although ALMT4 can mediate vacuolar uptake of these substrates in electrophysiological experiments, our phenotypic data argue against an anion uptake function for ALMT4, at least in guard cells. This is further supported by the fact that mutants transformed with the active ALMT4 S382A showed impaired stomatal opening. Therefore, we propose that ALMT4 is responsible for Mal^{2-} efflux during stomatal closure, a function that has not been characterized so far. ALMT4 might also mediate efflux of Fum^{2-} but there is little evidence for a role for Fum^{2-} in guard cells.

Although we have identified a role in guard cells, we cannot exclude that ALMT4 has additional functions in other cell types and organs since ALMT4 is expressed throughout the plant. The S382A growth phenotype is likely a result of the permanently reduced stomatal aperture causing reduced photosynthetic carbon assimilation and consequently growth. In addition, it might be caused by a reduced capability to store Mal^{2-} and Fum^{2-} in mesophyll vacuoles and, hence, generally impaired turgor-driven expansion growth. The growth phenotype could also be a result of reduced root growth due to impaired dicarboxylate storage or release for respiration. Both Mal^{2-} and Fum^{2-} are tricarboxylic acid cycle intermediates that accumulate during the day and are used for respiration during the night (Gago et al., 2016). Hence, in mesophyll tissue, release of Mal^{2-} and Fum^{2-} from the vacuole for respiration during the night might be a further important function of ALMT4. Although we could rule out an ALMT4 function in germination (Supplemental Figures 7A and 7B), one could envisage that ALMT4 is important during fertilization. Given its expression in flowers, it may regulate turgor or intracellular pH during pollen tube growth. Although we have focused on the role of Mal^{2-} as a charge-balancing counter ion and osmoticum during stomatal

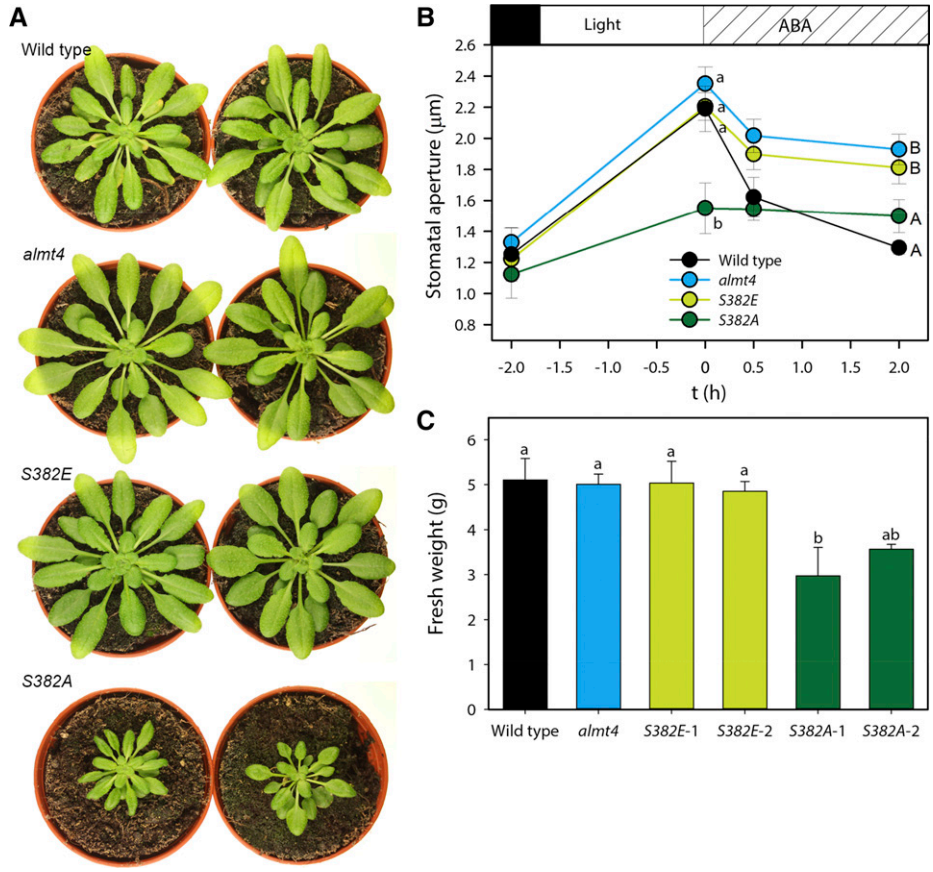

Figure 7. Stomatal Aperture Response and Rosette Growth of *almt4* Knockout Lines Transformed with Full-Length ALMT4 S382A (*S382A*) and S382E (*S382E*).

(A) Representative images of wild-type, *almt4*, *S382E*, and *S382A* plants.
(B) Epidermal peels of wild-type (black), *almt4* (blue), *S382E* (light green), and *S382A* (dark green) plants. Stomatal aperture was measured from dark-adapted plants, after a 2-h incubation under white light and subsequent 0.5- and 2-h incubations with 20 µM ABA. Data points are means of five different plants using 60 stomata per plant and significance of differences was tested between lines within one time point.
(C) Fresh weight of 6-week-old wild type, *almt4*, and two independent lines transformed with full-length ALMT4 S382A (*S382A-1* and *S382A-2*) and S382E (*S382E-1* and *S382E-2*), respectively ($n = 6$).
Data are means ± SE. Significant differences were determined using ANOVA followed by multiple comparison (at least $P \leq 0.05$) and are indicated by different letters.

regulation, ALMT4-mediated Mal^{2-} fluxes might contribute to maintaining cytoplasmic pH, which is crucial during pollen tube growth (Michard et al., 2017; Lovy-Wheeler et al., 2006). Furthermore, Mal^{2-} can act as a signaling molecule, activating Cl^- uptake through ALMT9 (De Angeli et al., 2013). A de-regulation of cytosolic Mal^{2-} concentration might hamper vacuolar Cl^- uptake, causing toxicity effects or altering the vacuolar membrane potential throughout the plant.

Potential Mechanism of ALMT4 Function during Stomatal Closure

In this study, ALMT4 is implicated in stomatal closure in response to ABA and drought stress, but not in response to darkness. This pattern hints that ALMT4 is part of an ABA-specific signaling pathway. Unlike ALMT6, ALMT4 does not depend on cytosolic Ca^{2+} and stomata of the *almt4* mutant closed normally in response to external Ca^{2+}. ABA-induced closure comprises a Ca^{2+}-dependent and a Ca^{2+}-independent pathway (Munemasa et al., 2015). Our data suggest that ALMT4 is either a target of Ca^{2+}-independent ABA signaling or that this channel is an upstream component in Ca^{2+}-dependent signaling. The latter could be the case if ALMT4 function leads to a change in tonoplast membrane voltage, causing Ca^{2+} efflux from the vacuole to generate cytosolic Ca^{2+} signals. As part of Ca^{2+}-independent signaling, ALMT4 could be the target of Ca^{2+}-independent kinases or phosphatases. However, there is also no indication of involvement of the core ABA-kinase OST1 in ALMT4 regulation. Instead, ALMT4 was inactivated when an in vivo phosphorylated serine was mutated to a phosphomimetic glutamate. This suggests that ALMT4 is regulated by ABA and de/phosphorylation through as yet unknown signaling pathways.

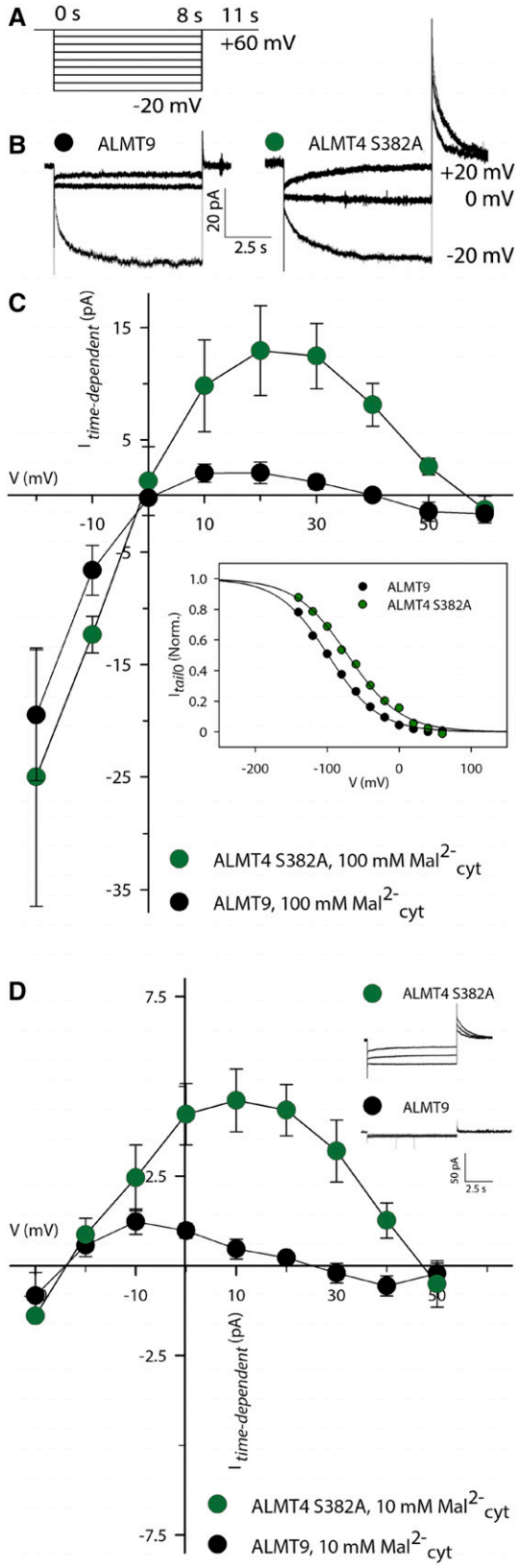

Figure 8. Analysis of ALMT4 S382A Outward Mal^{2-} Current.

The sequence of events allowing net solute loss from the guard cell in response to ABA has been well established mainly as regards events at the plasma membrane (Munemasa et al., 2015); however, little is known about how ABA regulates solute loss from the vacuole. K^+ efflux has been suggested to represent an early step in ABA-mediated changes at the vacuolar membrane (MacRobbie, 1995a, 1995b, 2000; Kollist et al., 2014), and it is mediated by channels of the two pore K^+ (TPK) channel family, in particular TPK1 (Gobert et al., 2007). K^+ efflux from the vacuole would lead to a depolarization of the vacuolar membrane potential. Depolarization would favor anion efflux, along their cytosol-directed concentration gradient. Despite the low vacuolar pH (~5.8 in Arabidopsis; Andrés et al., 2014), the largest part of malate is present as Mal^{2-} and hence gives rise to an outwardly directed Mal^{2-} concentration gradient (Meyer et al., 2011; Gerhardt and Heldt, 1984). If ALMT4 were open at all voltages, the direction of Mal^{2-} flux would depend solely on its electro-chemical gradient. The Nernst potential resulting from that gradient indicates the voltage at which the direction of flux reverses, the reversal potential. Based on Mal^{2-} concentration measurements and simulations (Martinoia and Rentsch, 1994; Gerhardt and Heldt, 1984; Chen et al., 2012; Hills et al., 2012), the physiological reversal potential for Mal^{2-} will be negative, probably around −30 mV. Hence, Mal^{2-} efflux can be expected for voltages positive of this potential if the channel is open at more positive voltages. The shift in ALMT4 open probability by more than 20 mV to more positive voltages compared with ALMT9 can therefore explain its ability to mediate Mal^{2-} efflux. Furthermore, the higher Mal^{2-} outward currents in ALMT4 compared with ALMT9, and the lower respective inward currents can be explained by the drastically increased ALMT4 rectification rate. This is illustrated in our working model (Figure 10): In response to a shift in vacuolar membrane voltage, ALMT9 closes thereby ceasing anion uptake. However, ALMT4 is still open and, since at more depolarized voltages the

(A) Schematic representation of the voltage protocol used. Activating currents were evoked by successive voltage pulses ranging from a holding voltage of +60 mV to −20 mV and recorded for 8 s, with successive voltage pulses increasing by 10 mV. Deactivating tail currents were recorded for 3 s by a subsequent step to holding voltage.

(B) Representative current traces of ALMT9 (black) and ALMT4 S382A (dark green) in symmetric Mal^{2-} conditions. For clarity, currents at −20 mV, 0 mV, and +20 mV are shown.

(C) I-V curve of ALMT4 S382A (dark green circles, $n = 7$) and ALMT9 (black circles, $n = 8$) time-dependent currents at steady state in symmetric Mal^{2-} conditions (green and black circles, 100 mM Mal^{2-}_{vac}/100 mM Mal^{2-}_{cyt}). Inset: Tail current amplitudes of open channel current (I_{tail0}) normalized to the respective maximum I_{tail0} of ALMT9 (black circles) and active ALMT4 S382A (dark green circles). Data are representative and were fitted with the Boltzman function (black lines; Supplemental Figure 5; see Methods). Averages of derived gating parameters are shown in Table 1.

(D) I-V curve of ALMT4 S382A (dark-green circles, $n = 7$) and ALMT9 (black circles, $n = 5$) time-dependent currents at steady state in asymmetric Mal^{2-} conditions (100 mM Mal^{2-}_{vac}/10 mM Mal^{2-}_{cyt}) and representative current traces (inset).

Currents were measured on excised outside-out patches of *N. benthamiana* vacuoles, confirmed to express ALMT4 S382A-GFP and ALMT9-GFP. Data points are means of current means at steady state. Error bars denote the SE.

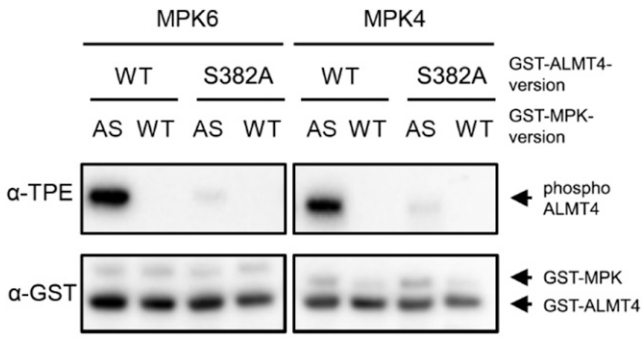

Figure 9. In Vitro Phosphorylation of ALMT4 S382 by MPK6 and MPK4.

Thiophosphorylation assays of GST-tagged native and phosphosite S382A mutant C-terminal ALMT4. GST-ALMT4^{WT} (WT) and GST-ALMT4^{S382A} (S382A) were incubated in the presence of Bn-ATPγS as cofactor with GST-MPK4 or GST-MPK6 (see Methods). The GST-MPK recombinant proteins used were sensitive to Bn-ATPγS as a thiophosphate donor (analog-sensitive [AS]) or were wild type, as a negative control. Phosphorylated ALMT4 (phosphoALMT4) was visualized by an anti-thiophosphate ester-specific antibody (α-TPE), and the GST fusion proteins were visualized by an anti-GST antibody (α-GST) to test for equal loading.

Mal^{2-} reversal potential favors efflux, ALMT4 mediates anion loss from the vacuole. In this study, we show that ALMT4 is also involved in inhibition by ABA of stomatal opening. Presumably ABA leads to ALMT4 activation, leading to Mal^{2-} efflux, counteracting Mal^{2-} influx by other transporters. Possibly, ALMT4 carries more than one function and it might additionally halt uptake of anions through other ALMT channels via subunit interaction (Hille, 2001; Zhang et al., 2013; Geiger et al., 2009; Zheng, 2013).

Although current amplitudes decreased when an outward-directed Mal^{2-} concentration gradient was applied in patch clamp experiments, the difference in outward current between ALMT4 and ALMT9 was consistent. The amplitude decrease could not be explained by a Mal^{2-} dependence of channel open probability, as is the case for some K^+ channels (Blatt, 1988; Johansson et al., 2006). Although larger time constants for current activation might in part explain the decreased outward current amplitudes, interacting ions or proteins might also influence ALMT4 activity. However, in our experiments, the vacuolar membrane is isolated from any cytosolic and vacuolar contents and the resulting absence of potential interacting or modulating factors might explain the observed current decrease.

Regulation of ALMT4 by Phosphorylation

Regarding ALMT4 function in stomata, our results with phosphomimic and dephosphomimic mutants suggest that the resting state of the channel is phosphorylated and that it becomes active through dephosphorylation when ABA-dependent stomatal closure occurs. According to our electrophysiological results, channels in the *S382E* lines would be constitutively inactive. This would explain why these lines display *almt4* mutant-like stomatal behavior. The transformants expressing a constitutively active channel (*S382A*) show drastically impaired opening. A phosphorylation-induced inactivation of the channel during stomatal opening would explain why ALMT4, which is present in the *almt9* mutant that displays impaired stomatal opening, cannot compensate for the lack of ALMT9. One could speculate that S382 is dephosphorylated only during short, specific times, maybe in response to drought stress, whereas phosphorylation might represent a more constitute deactivation, preventing efflux during stomatal opening.

Here, we provide in vitro data indicating that ALMT4 might be phosphorylated and deactivated by MPKs. Typically, MAP kinase signaling comprises a cascade of three kinases (Lee et al., 2016). In 2011, it was shown that VIK of Arabidopsis, a MAP kinase kinase, also directly interacts with a vacuolar transport protein (Wingenter et al., 2011). The authors showed that VIK interacted with and stimulated the glucose uptake activity of the TONOPLAST MONOSACCHARIDE TRANSPORTER1. MPKs are not known to be part of the core ABA-signaling network, but more and more evidence is emerging that implicates MAP kinases in biotic and

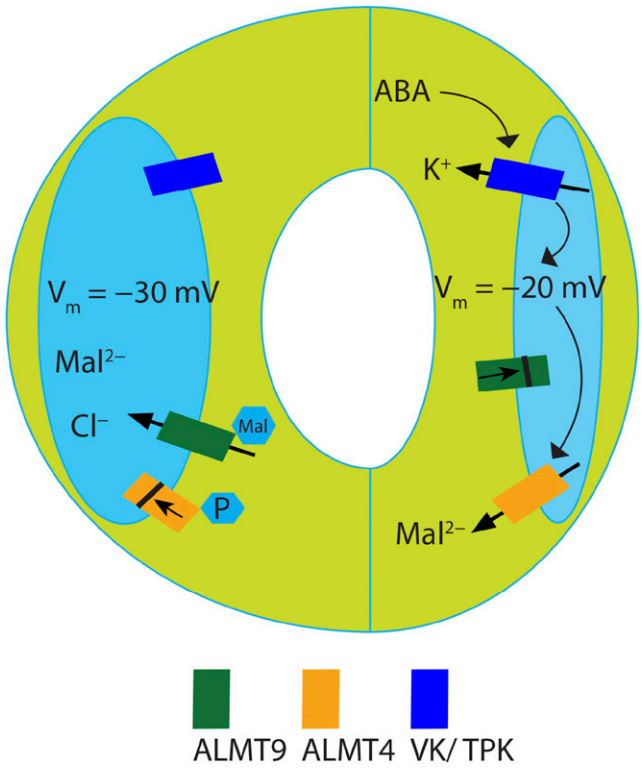

Figure 10. Model of ALMT4 Function in Stomatal Closure.

Other (not all) identified conductances at the vacuolar membrane that contribute to stomatal opening and closing are also depicted (VK/TPK = vacuolar K^+ channel/two-pore K^+ channel). Events hypothetically taking place in response to ABA are depicted by black arrows. During stomatal opening (left), vacuolar uptake of Cl^- is facilitated through ALMT9, while ALMT4 is phosphorylated and inactive. During stomatal closure (right) in response to ABA, the vacuolar K^+ conductance is activated causing a depolarization of the vacuolar membrane potential, which leads to ALMT9 channel closure and cessation of solute uptake. ALMT4 is dephosphorylated by an unknown phosphatase and active. Since active ALMT4 is open at more positive voltages than ALMT9 it can mediate Mal^{2-} efflux at more depolarized tonoplast potentials.

abiotic stress signaling during stomatal movement (Lee et al., 2016; de Zelicourt et al., 2016; Jakobson et al., 2016; Hõrak et al., 2016; Su et al., 2017). However, no MAP kinase ion channel substrates involved in stomatal movement have been identified. Here, we show that ALMT4 might be an in vivo substrate of MPKs. To date, MPK9 and MPK12 are known to be required for ABA-induced stomatal closure through activation of the SLAC1 anion efflux channel (Jammes et al., 2009; Lee et al., 2016). Also, *Nicotiana attenuata* deficient in *Na*MPK4 was impaired in ABA-induced stomatal closure (Hettenhausen et al., 2012). In addition, MPK12 and MPK4 of Arabidopsis interact with and inhibit the CO_2-responsive kinase HT1, causing SLAC1 activation and stomatal closure in response to high CO_2 (Jakobson et al., 2016; Hõrak et al., 2016). Therefore, MPK4 and MPK12 are unlikely to be required for ALMT4 inactivation during stomatal opening. Instead, our data suggest that a potential MAP kinase acting on ALMT4 would counteract closure and that it might be inactivated by ABA. Despite many studies showing *mpk* mutants to be impaired in stomatal closure, MPK6 is an example where a MAP kinase is *NOT* required for stomatal closure in response to ABA (Montillet et al., 2013); conversely, a dominant-negative MPK6 mutant was hypersensitive to ABA (Leung et al., 2006). However, MPK6 is required for stomatal closure in response to the bacterial elicitor flagellin (Montillet et al., 2013; Su et al., 2017) and it is required, in redundance with MPK3, for stomatal immunity involving altered organic acid metabolism (Su et al., 2017). In line with the results on ABA response in *mpk6* mutants, it was recently shown that ABA inactivated MPK6 (Mine et al., 2017). MPK6 is activated upon bacterial infection, during both pattern-triggered and effector-triggered immunity. Some pathogens, such as *Pseudomonas syringae* pv *tomato* (*Pto*) DC3000, counteract immunity by activating, among others, ABA signaling, and ABA has been known to negatively impact immunity against *Pto* DC3000 (de Torres Zabala et al., 2009). Mine et al. (2017) showed that ABA induced the expression of HAI phosphatases of the PP2C (protein phosphatase 2C)-type, which in turn inactivate MPK6 through dephosphorylation. Thus, one could speculate that active MPK6 shuts down ALMT4 in the ground state but that this kinase is inactivated in response to ABA, thus ceasing ALMT4 phosphorylation, causing Mal^{2-} efflux. However, while our data show that MPK6 can phosphorylate ALMT4 in vitro, it cannot be excluded that another MPK is involved in this process, and it is a challenge for the future to pinpoint the exact kinases and phosphatases involved in ALMT4 regulation in vivo.

Conservation of ALMT4 S382 among ALMT Channels

Mutation of S382 has a striking effect on ALMT4 current activity and plant growth, and phosphorylation of this site seems to act in a deactivating manner. To investigate if this site is conserved among clade II ALMTs, we performed an amino acid sequence alignment (Supplemental Figure 8). Interestingly, S382 is conserved only in ALMT5, but here the serine is not followed by proline. Therefore, proline-directed phosphorylation of S382 in clade II ALMTs seems to be unique to ALMT4. This is in line with our observation that ALMT9, which does not feature a phosphorylatable serine in the vicinity of the identified motif, did not show discernible outward Mal^{2-} currents and *almt9* knockout mutants showed wild-type-like stomatal closure in response to ABA (De Angeli et al., 2013). Interestingly, however, the SP dipeptide motif was conserved in ALMT12. ALMT12, like ALMT4, is involved in stomatal closure and mediates anion efflux from the guard cell. A site-directed mutagenesis screen of ALMT12 electrophysiological properties had been conducted previously to identify putative regulatory C-terminal serines (Mumm et al., 2013). In this screen ALMT12 C-terminal serines were mutated to alanine with the reasoning that if they were phosphorylated, the S-to-A mutation would deactivate the channel. However, these mutations did not shut down channel activity. In light of our results, these serines and the ALMT12 S382A homolog might bear importance nonetheless but phosphorylation might deactivate the channel rather than activate it. It is therefore tempting to speculate that ALMT4 and ALMT12 act in concert during drought stress-induced stomatal closure and that this relies on dephosphorylation, rather than phosphorylation. Although, in guard cells, many ion channels and transporters are activated by phosphorylation, there are some exceptions such as the inward-rectifying K^+-channel and the plasma membrane H^+-ATPase (Fuglsang et al., 2007; Sato et al., 2009). Phosphorylation can also target proteins for degradation; however, our GFP-tagged phosphomimetic channel mutant construct yielded strong fluorescence at the vacuolar membrane, comparable to that of the wild type. Therefore, in light of our results, the localization and stability of ALMT channels involved in stomatal closure are not likely to be modulated by phosphorylation/dephosphorylation but the channel might be activated by dephosphorylation.

METHODS

Molecular Biology

ALMT4 (At1g25480) cDNA was amplified from Col-0 rosette leaf cDNA and cloned into the binary expression vector pART27 (Gleave, 1992) using primers including overhangs for *Xho*I and *Kpn*I restriction sites at the 5′ and the 3′ end, respectively, as well as excluding the stop codon and including a 3′ seven-amino acid linker (sense, 5′-TCAGATCGCTCGAGATGGCTGACCAAACTAGAG-3′; antisense, 5′-CGGTACCAGATCCAGCAGCACCTCCAGATATCCGTGTCTCGCTAAC-3′). The pART27 construct contained *GFP* at the 3′ end and in frame with *ALMT4* and was used for localization and patch-clamp experiments. *ALMT4* complementation constructs were cloned using ligation-independent cloning (LIC) into pPLV22 (De Rybel et al., 2011), which contained a tandem-tomato fluorescent marker in frame at the 3′ end of the inserted complementation construct. For this, a fragment containing a 1837-bp sequence upstream of the *ALMT4* start codon as well as the complete genomic DNA excluding the stop codon was amplified from Col-0 leaf genomic DNA. Primers with LIC-compatible overhangs were used (sense, 5′-TAGTTGGAATGGGTTCGAAGTTTCTCTCACAGGATAA-3′; antisense, 5′-TAGTTGGAATGGGTTCGAAGTTTCTCTCACAGGATAA-3′). To generate the $ALMT4_{Pro}$:GUS construct, the 1837-bp promoter sequence upstream of the start codon of *ALMT4* was cloned into pMDC163 (Curtis and Grossniklaus, 2003). The primers that were used to amplify the *ALMT4* promoter region were as follows: sense, 5′-GGGGACAAGTTTGTACAAAAAAGCAGGCTTAGTTTCTCTCACAGGATAA-3′; and antisense, 5′-GGGGACCACTTTGTACAAGAAAGCTGGGTGTTGCGTTGATTTCTTCTTCC-3′.

Site-directed mutagenesis was performed on the pART27 expression and pPLV22 complementation constructs according to Zhang et al. (2013)

using primers for the S382A mutation (sense, 5′-AGAAGCTAGCTC-CAGGGAACGTT-3′; antisense, 5′-TTCCCTGGAGCTAGCTTCTCCAT-3′) and for the S382E mutation (sense, 5′-AGAAGCTAGAGCCAGGGAACGTT-3′; antisense, 5′-TTCCCTGGCTCTAGCTTCTCCAT-3′), respectively.

For expression of GST-ALMT4^{WT} in *Escherichia coli*, *ALMT4* was amplified from cDNA by PCR using oligonucleotide primers ALMT4^{320} (sense, 5′-GGATCCCCGCTGGAGAAGACCTCCATAAAC-3′) and ALMT4^{548} (antisense, 5′-GAATTCCTATATCCGTGTCTCGCTAACTTG-3′). Next, the PCR-product was digested with *Bam*HI and *Eco*RI and ligated in plasmid pGEX-5X-3 (GE Healthcare). To generate GST-ALMT4^{S382A}, site-directed mutagenesis was performed according to the instructions of the QuickChangeII site-directed mutagenesis kit (Stratagene).

Knockout lines for *ALMT4* (see section below) were genotyped using T-DNA left border primers (SALK, 5′-ATTTTGCCGATTTCGGAAC-3′; RIKEN, 5′-TACCTCGGGTTCGAAATCGAT-3′) and gene-specific primers for SALK_086236 (left primer, 5′-TTCGATCAAATCTTCCGGATTT-3′; right primer, 5′-CTTCAAGTGAATTGGCCACAC-3′), and for RATM13-0411-1_G/PST (left primer, 5′-GCATTCAGGGTGTTTTTGTTG-3′; right primer, 5′-AAACATCTTTTATGGACGGCC-3′). Genotyping was performed using the KAPA3G plant PCR kit (KAPA Biosystems) according to the manufacturer's instructions.

Plant Growth, Transformation, and Selection

Arabidopsis thaliana plants were grown in controlled environment chambers (HIROSS; Klimatec) at short-day (8 h light/16 h dark, 60% relative humidity (RH), 21°C) or long-day (16 h light/8 h dark, 60% RH, 21°C) conditions for physiological experiments. Plants were grown under a white light spectrum generated by four fluorescent lamps, three Osram Biolux 36W/965 or 58W/965 lamps, and one Osram Fluora 36W/77 or 58W/77 lamp. For propagation, plants were grown in the greenhouse. Data from plant lines that were compared in any one experiment were always grown from seeds that were harvested together from plants grown at the same time, under the same conditions. Seeds were sown onto moist soil (Einheitserdewerke Patzer) and vernalized at 4°C for 48 h. After 10 to 14 d, seedlings were transplanted into individual pots.

Arabidopsis was transformed using the floral dip method (Clough and Bent, 1998) according to Zhang et al. (2006). Transformants with pPLV22 constructs carried the *bar* gene and seeds were sown onto soil in a lawn-like fashion and treated with BASTA (150 μM; Omya) three times every 2 to 3 d, 14 d after germination. Resistant seedlings were transferred into individual pots and propagated.

Two independent knockout lines of *ALMT4* were ordered from NASC (The European Arabidopsis Stock Centre, Loughborough, UK): a T-DNA insertion line in the Columbia-0 (Col-0) background (SALK_086236) with the flanking sequence in the third exon (Alonso et al., 2003), and a Ds transposon mutant in the Nossen-0 (No-0) background (RATM13-0411-1_G/PST) with the flanking sequence in the first exon (Ito et al., 2002). From heterozygous parents, individuals of each line were genotyped as described above and a homozygous knockout as well as homozygous wild type outcrosses were selected for each line. Thus, in case of any undetected T-DNA or transposon insertions, the wild type will have a corresponding genetic background to the mutant.

Intracellular Localization

Nicotiana benthamiana were transformed with the ALMT4-GFP construct. Three to five days after transformation, protoplasts and isolated vacuoles were obtained as described in the "Patch-Clamp Experiments" section. Samples were imaged using a Leica TCS SP5 confocal microscope (Leica Microsystems). GFP fluorescence was excited using a 488-nm laser, with GFP and chlorophyll fluorescence being collected between 500 to 600 nm and 698 to 787 nm, respectively.

GUS Staining

ALMT4 promoter activity was analyzed in three independent transgenic lines expressing ALMT4$_{Pro}$:GUS. Plants were grown on soil in short-day conditions, for 3 weeks. For GUS staining, whole plantlets were vacuum infiltrated and incubated for 3 h at room temperature with a staining solution containing 1 mM X-Gluc (5-bromo-4-chloro-3-indolyl-β-D-glucuronide) in 50 mM sodium phosphate buffer, pH 7.15, 0.5 mM potassium ferricyanide, 0.5 mM potassium ferrocyanide, and 0.05% Triton X-100. The tissue was washed three times in 50 mM sodium phosphate buffer, pH 7.15, and cleared overnight at 37°C with 70% ethanol.

Expression Analysis

For the expression analysis of *ALMT4*, plants were grown under long-day conditions, either on plates for mRNA level determination in seedlings or in sterile cylinders for all other tissue. The plates and cylinders contained 0.5× Murashige and Skoog medium, pH 5.6, and 1% phytoagar. Seedlings were 7 d old when harvested. In all other tissue, the expression levels were determined in 7-week-old plants. In addition, dry seeds were used for analysis of *ALMT4* transcript abundance. Two biological replicates were performed, in each of which material of five plants was pooled.

For expression analysis of clade II *ALMT* members, *almt4* (Col-0) mutants and the appropriate wild-type plants were grown in a hydroponic culture for four weeks at 16 h light/8 h dark, 60% RH, 21°C. The 0.5× Murashige and Skoog medium, pH 5.6, was used as nutrient solution. For each genotype, a whole rosette was harvested, and two separate replicate experiments were performed.

Total RNA was extracted using the SV Total RNA Isolation System (Promega) and reverse transcribed using the M-MLV reverse transcriptase (Promega) according to the manufacturer's instructions. Transcript levels were determined by qRT-PCR using the 7500 Fast Real-Time PCR System (Applied Biosystems) and a SYBR Green PCR Master Mix (Applied Biosystems). Transcript levels were calculated with the standard curve method as described by Pfaffl (2001) and were normalized against the expression of the actin gene *ACT2*. We used primers for *ACT2* (sense, 5′-TGGAATCCACGAGACAACCTA-3′; antisense, 5′-TTCTGTGAACGATTCCTGGAC-3′), *ALMT9* (sense, 5′-ACCTAATCCGGA-TCTTAGTCGATACT-3′; antisense, 5′-TCACCGAATAAAGTGGAAAGCTCAG-3′), *ALMT6* (sense, 5′-CCGTTGCATGATGCTAGTAAATAC-3′; antisense, 5′-TGATGATGGTTTGCTCGAAA-3′), *ALMT5* (sense, 5′-GAGCCGCTT-CAAGATGCTAGTA-3′; antisense, 5′-ATGACTTCTTCAAACTCTCCTGCT-3′), *ALMT4* (sense, 5′-TGACGCTAGCAAGTATGCTGTT-3′; antisense, 5′-CTTCAAATTCTCCAGCTGAAACAGA-3′), and *ALMT3* (sense, 5′-GGCTTATCCTACAGAGCAGAGGCT-3′; antisense, 5′-TCAGAGCCAAAC-CCATCTTC-3′). All reactions were performed in technical triplicates that were averaged to generate a biological replicate.

Stomatal Experiments

Plants were grown under short-day conditions for 6 weeks and then transferred to an LED-controlled environment chamber (Fytoscope FS130; Photon Systems Instruments) and adapted at 250 μmol m^{-2} s^{-1} white light (12 h light/12 h dark) for 3 d. Before the experiment, the plant genotypes were blinded to avoid experimenter bias. Epidermal peels were obtained 1 h before the start of the light period in green light from young but fully expanded rosette leaves. Peels from at least four different plants per genotype were incubated in opening buffer (10 mM MES-KOH, pH 6.1, 0.1 mM $CaCl_2$, and 30 mM KCl) in custom-built imaging chambers. To avoid chamber effects, each incubation chamber contained peels from all genotypes compared in any one experiment. After imaging in the dark, peels were incubated in 250 μmol m^{-2} s^{-1} white light for 2 h and imaged again. If required, the opening buffer was supplemented with 20 μM ABA to investigate ABA-mediated inhibition of stomatal opening. To induce

stomatal closure, peels were treated with 20 μM ABA or 1 mM $CaCl_2$ in opening buffer, returned to the light, and imaged over a 2-h time course at indicated times. Three images were obtained from each peel at each time point using an inverted Eclipse TS 100 microscope fitted with a Plan Fluor 40×/0.75 objective and a Digital Sight DS-Fi1 camera (Nikon). Finally, recorded images were blind-analyzed using ImageJ (Abràmoff et al., 2004), and the apertures of 60 stomata were measured per leaf. Mean apertures of a single leaf were averaged over at least four leaves measured per genotype.

Gas Exchange Measurements

Plants were grown in short-day conditions for 4 to 5 weeks and measured using an LI-6400XT infrared gas analyzer fitted with an LI-6400-17 whole-plant Arabidopsis chamber (LI-COR Environmental). Plants were adapted to chamber conditions (22°C block temperature, 55% RH, 400 ppm CO_2) in the dark for 1 h prior to measurement.

Drought Stress and RWC Measurements

Plants were germinated in short-day conditions for 14 d and transplanted into individual pots, filled with 75 g ± 1 g sieved soil, and soaked in water overnight. Genotypes were randomly distributed on growth trays and plants were grown for 2 weeks before watering was stopped and the soil sealed with black plastic wrap to avoid evaporation. After 6 weeks, plants showed obvious signs of wilting, and from each plant the 12 youngest but fully expanded rosette leaves were harvested and sealed in a preweighed plastic zipper bag before fresh weight determination. Harvesting occurred from all genotypes within 1 h of solar noon. Subsequently, 10 mL of 5 mM $CaCl_2$ in double-distilled water was added to the zipper bags to allow leaves to rehydrate overnight in the dark. Rehydrated leaves were patted dry and their turgid weight was determined. They were then dried at 60°C for 72 h before dry weight determination and RWC was calculated according to Equation 1:

$$RWC = \frac{(FW - DW)}{(TW - DW)} \times 100\% \quad (1)$$

where FW is the fresh weight, DW is the dry weight, and TW is the turgid weight.

Water Loss Experiments

Fully expanded rosette leaves were harvested, their fresh weight was recorded, and their petioles were incubated either in 20 μM ABA or in a control solution (double distilled water with 0.2% ethanol) in white light for 1 h. They were then left to air-dry for 7 h, their fresh weight was recorded and normalized to the initial value, and the difference was expressed as percentage of water loss.

Patch-Clamp Experiments

For patch-clamp analysis, we transiently transformed *N. benthamiana* with *Agrobacterium tumefaciens* harboring ALMT4-GFP, ALMT4 S382A-GFP, ALMT4 S382E-GFP, and ALMT9-GFP constructs using the agroinfiltration method (Sparkes et al., 2006). Experiments were performed 4 to 7 d after transformation, and expression of each fusion protein at the vacuolar membrane was confirmed before each patch (see below for microscope description).

Transformed *N. benthamiana* leaves were digested in digest solution (10 mM MES, pH 5.3 adjusted with KOH, 1 mM $CaCl_2$, 500 mM sorbitol, 0.3% [w/v] Cellulase "Onozuka R-10" [Serva], 0.03% (w/v) Pectolyase Y-23 [Kyowa Chemical Industry]) for 35 min at 30°C. Protoplasts were washed twice in digest solution without enzymes and were allowed to settle by gravity for 10 to 20 min on ice. Protoplasts were kept on ice for 2 to 3 h, during which time aliquots were transferred onto a custom-built measuring chamber and perfused with standard Mal^{2-} bath solution (100 mM malic acid, 1 mM $CaCl_2$, pH adjusted with Bis-Tris propane to pH 7.5, osmotic content adjusted to 500 mosmol/ kg with sorbitol) in order to release vacuoles. Borosilicate thin-wall capillaries (30-0062) for patch pipettes were obtained from Harvard Apparatus. Capillaries were internally coated with Sigmacoat overnight at 60°C and patch pipettes were prepared using a P-30 Micropipette Puller (Sutter Instrument Company) to give a resistance of 5.5 MΩ ± 0.3 MΩ with standard Mal^{2-}-based bath and pipette solutions. Finally, pipette tips were coated with silicone (Sylgard 184 Silicone Elastomer Kit; Dow Corning) to reduce pipette capacitance.

For measurements, pipettes were filled with standard pipette solution (112 mM malic acid, 10 mM HCl, 1 mM $CaCl_2$, adjusted with Bis-Tris propane to pH 6, osmotic content adjusted to 550 mosmol/ kg with sorbitol). Pipettes were mounted onto a HEKA amplifier headstage connected to a HEKA EPC 10 USB amplifier (HEKA Elektronik Dr. Schulze). A 3 M KCl/ 0.1% agarose bridge served as a reference electrode. The measuring chamber and micromanipulator were fitted onto an Eclipse *Ti* inverted microscope fitted with Plan Fluor 20×/0.45 and 40×/0.6 objectives (Nikon). GFP fluorescence was excited using a CoolLED p-100 and emission collected using a F36-525 EGFP HC filter set (Semrock; AHF). Seals between vacuolar membrane and the pipette were created and, if they were larger than 2 GΩ, access was established by application of a 0.5 ms 700 mV pulse and parallel application of underpressure through suction. After break-in, an outside-out membrane patch was excised. The membrane patch was perfused with standard bath solutions, referred to as cytoplasmic solutions, and were exchanged for different bath solutions as required. When the Mal^{2-} concentration was changed, the bath solution osmotic content was adjusted accordingly, and the ionic strength was adjusted with MES. For measurements with other substrates, the bath and pipette solutions were as described for standard solution but the charge carrying or activating ion was replaced at the indicated concentrations. In all experiments, the measured liquid junction potential was below 1 mV and therefore no correction was applied. Currents were recorded with a 1-kHz sampling interval, filtered at 0.3 kHz using the Patchmaster software (HEKA), and analyzed using Fitmaster (HEKA).

In Vitro Kinase Assay

Substrate-labeling reactions were performed essentially as described (Leissing et al., 2016). In brief, 100 ng activated recombinant wild-type or analog-sensitive GST-MPKs were mixed with 1 μg of GST-$ALMT4^{WT}$ or GST-$ALMT4^{S382A}$ in kinase reaction buffer (50 mM Tris-HCl, pH 7.5, 10 mM $MgCl_2$, and 1 mM DTT) including 1 mM N6-Bn-ATPγS (Biolog). Each 30-μL reaction was stopped by adding 20 mM EDTA after 1 h and the thiophosphorylated substrate was alkylated with 2.5 mM *p*-nitrobenzyl mesylate (Abcam) in 5% (v/v) DMSO for 2 h. The alkylation reaction was mixed with SDS loading buffer before samples were subjected to SDS-PAGE and transferred to a nitrocellulose membrane (Carl Roth). Immunodetection was performed using the rabbit monoclonal antibodies against the thiophosphate ester (α-TPE; Abcam) to detect thiophosphorylated kinase substrates. Rabbit α-GST (CST) served to check for equal gel loading. Antigen-antibody complexes were detected with horseradish peroxidase-coupled anti-rabbit secondary antibodies (CST) followed by chemiluminescence detection with Luminata Crescendo HRP substrate (Millipore). Using independent protein preparations, all substrate thiophosphorylation reactions were repeated at least twice with similar results.

Analysis of State Transition Rate Time Constants

Macroscopic voltage-dependent current kinetics can be derived from voltage-clamp experiments (Supplemental Figure 5) where each activating

voltage step (e.g., from + 60 mV to –100mV) is followed by a deactivating voltage step (e.g., from –100 mV to + 60 mV). The activation kinetics of the current in response to the voltage step informs on the reaction rate of the closed to open channel state transition. Conversely, the kinetics of the ionic currents in response to the deactivating pulse reflects the reaction rate of open to closed channel state transition. During this deactivating pulse until the channels are closed they conduct an outward current since the electrochemical gradient has reversed together with the transmembrane voltage. The currents measured during a deactivating voltage step are called tail currents. Since activating and deactivating current kinetics reflect state transition reactions, they can be fitted by exponential functions (Supplemental Figure 5) to derive time constants (τ) that inform on the rates of the state transitions.

Boltzman Analysis

In I-V curve recordings, the current at the start of each deactivating voltage step (I_{tail0}; Supplemental Figure 5) is proportional to $P_o rel$ of the channel at the end of the previous activation pulse (Equation 2). We analyzed the $P_o rel$-to-voltage relationship using a Boltzman function (Equation 3) and derived gating parameters, the half-maximal activation voltage ($V_{1/2}$), and the gating charge (z_g). The rational of the analysis is illustrated in Supplemental Figure 5.

$$I_{tail\,0} = N \times i \times P_o rel \times V_m \quad (2)$$

where $I_{tail\ 0}$ is the tail current amplitude at the start of the deactivating voltage pulse, N is the number of channels contributing to macroscopic current, i is the single channel conductance, $P_o rel$ is the relative open probability at the activation pulse, and V_m is the membrane voltage.

$$I_{tail\,0} = \frac{I_{tail\,0}max}{1 + e^{\,z_g \times \frac{F}{RT} \times (V - V_{1/2})}} \quad (3)$$

where $I_{tail\ 0}$ is the tail current amplitude at the start of the deactivating voltage pulse, V is the applied activation pulse voltage, $V_{1/2}$ is the half-maximal activation voltage, z_g is the gating charge, R is the universal gas constant, F is the Faraday constant, and T equaled 298.15K.

Statistics

The n numbers used for statistical analysis are given in the figures and tables. Data were tested for normal distribution. Normally distributed data were compared by Student's t test or, if more than two groups were compared, by ANOVA and a post-hoc test. If normality test failed, data were tested by ANOVA on ranks. Tests were conducted using SigmaPlot (Systat Software). Values from statistical analyses can be found in Supplemental File 1.

Chemicals

All chemicals were purchased from Sigma-Aldrich Chemie, AppliChem, or Roth unless stated otherwise.

Accession Numbers

Sequence data from this article can be found in the GenBank data library under accession numbers At1g18420 (*ALMT3*), At1g25480 (*ALMT4*), At1g68600 (*ALMT5*), At2g17470 (*ALMT6*), At3g18440 (*ALMT9*), At4g17970 (*ALMT12*), and AT3G18780 (*Actin2*).

Supplemental Material

Supplemental Figure 1. *ALMT4* mRNA expression analysis.

Supplemental Figure 2. Response of stomatal aperture to ABA (second experiment).

Supplemental Figure 3. Transpiration rate response over time of dark-adapted plants to light and dark.

Supplemental Figure 4. Current amplitude distribution.

Supplemental Figure 5. Illustration of Boltzman and tail current analysis.

Supplemental Figure 6. Stomatal response to ABA of S382 mutants (second independent line).

Supplemental Figure 7. Germination with and without ABA.

Supplemental Figure 8. Alignment of ALMT4 with clade II ALMT channels and ALMT12 from Arabidopsis.

Supplemental Table 1. ALMT4 S382A gating parameters in 100 and 10 mM Mal^{2-}.

Supplemental File 1. Tables of results from statistical analyses.

ACKNOWLEDGMENTS

We acknowledge Karl Huwiler and Christian Frey for help with plant maintenance and Daniel Bollier for technical support. We thank Dietmar Geiger (Würzburg) for the provision of OST1 constructs. C.E. was supported by the European Union's Seventh Framework Programme for research, technological development, and demonstration under grant agreement GA-2010-267243–PLANT FELLOWS and the University of Zurich Forschungskredit. U.B. and A.D.A. were supported by the Swiss National Foundation (31003A_141090/1) and University of Zurich Forschungskredit. G.J.M.B. was supported by the Deutsche Forschungsgemeinschaft (BE4054/2-1). J.Z. was a fellow of the Chinese Scholarship Council.

AUTHOR CONTRIBUTIONS

C.E., A.D.A., and E.M. designed the research. C.E., U.B., N.V.H., G.J.M.B., and J.Z. performed research. C.E., U.B., and G.J.M.B. analyzed data. C.E., A.D.A., G.J.M.B., and E.M. wrote the article.

Received June 9, 2017; revised August 9, 2017; accepted August 31, 2017; published September 5, 2017.

REFERENCES

Abràmoff, M.D., Magalhães, P.J., and Ram, S.J. (2004). Image processing with ImageJ. Biophotonics International **11:** 36–41.

Alonso, J.M., et al. (2003). Genome-wide insertional mutagenesis of *Arabidopsis thaliana*. Science **301:** 653–657.

Andrés, Z., Pérez-Hormaeche, J., Leidi, E.O., Schlücking, K., Steinhorst, L., McLachlan, D.H., Schumacher, K., Hetherington, A.M., Kudla, J., Cubero, B., and Pardo, J.M. (2014). Control of vacuolar dynamics and regulation of stomatal aperture by tonoplast potassium uptake. Proc. Natl. Acad. Sci. USA **111:** E1806–E1814.

Araújo, W.L., Nunes-Nesi, A., and Fernie, A.R. (2011). Fumarate: Multiple functions of a simple metabolite. Phytochemistry **72:** 838–843.

Baetz, U., Eisenach, C., Tohge, T., Martinoia, E., and De Angeli, A. (2016). Vacuolar chloride fluxes impact ion content and distribution during early salinity stress. Plant Physiol. **172:** 1167–1181.

Chia, D.W., Yoder, T.J., Reiter, W.-D., and Gibson, S.I. (2000). Fumaric acid: an overlooked form of fixed carbon in Arabidopsis and other plant species. Planta **211:** 743–751.

Chrispeels, M.J., Crawford, N.M., and Schroeder, J.I. (1999). Proteins for transport of water and mineral nutrients across the membranes of plant cells. Plant Cell **11:** 661–676.

Bertl, A., et al. (1992). Electrical measurements on endomembranes. Science **258:** 873–874.

Blatt, M.R. (1988). Potassium-dependent, bipolar gating of K^+ channels in guard cells. J. Membr. Biol. **102:** 235–246.

Chen, Z.-H., Hills, A., Bätz, U., Amtmann, A., Lew, V.L., and Blatt, M.R. (2012). Systems dynamic modeling of the stomatal guard cell predicts emergent behaviors in transport, signaling, and volume control. Plant Physiol. **159:** 1235–1251.

Chrispeels, M.J., Crawford, N.M., and Schroeder, J.I. (1999). Proteins for transport of water and mineral nutrients across the membranes of plant cells. Plant Cell **11:** 661–676.

Clough, S.J., and Bent, A.F. (1998). Floral dip: a simplified method for Agrobacterium-mediated transformation of *Arabidopsis thaliana*. Plant J. **16:** 735–743.

Curtis, M.D., and Grossniklaus, U. (2003). A Gateway cloning vector set for high-throughput functional analysis of genes in planta. Plant Physiol. **133:** 462–469.

De Angeli, A., Zhang, J., Meyer, S., and Martinoia, E. (2013). AtALMT9 is a malate-activated vacuolar chloride channel required for stomatal opening in Arabidopsis. Nat. Commun. **4:** 1804.

De Rybel, B., van den Berg, W., Lokerse, A., Liao, C.-Y., van Mourik, H., Möller, B., Peris, C.L., and Weijers, D. (2011). A versatile set of ligation-independent cloning vectors for functional studies in plants. Plant Physiol. **156:** 1292–1299.

de Torres Zabala, M., Bennett, M.H., Truman, W.H., and Grant, M.R. (2009). Antagonism between salicylic and abscisic acid reflects early host-pathogen conflict and moulds plant defence responses. Plant J. **59:** 375–386.

de Zelicourt, A., Colcombet, J., and Hirt, H. (2016). The role of MAPK modules and ABA during abiotic stress signaling. Trends Plant Sci. **21:** 677–685.

Ding, Z.J., Yan, J.Y., Xu, X.Y., Yu, D.Q., Li, G.X., Zhang, S.Q., and Zheng, S.J. (2014). Transcription factor WRKY46 regulates osmotic stress responses and stomatal movement independently in Arabidopsis. Plant J. **79:** 13–27.

Dreyer, I., Gomez-Porras, J.L., Riaño-Pachón, D.M., Hedrich, R., and Geiger, D. (2012). Molecular evolution of slow and quick anion channels (SLACs and QUACs/ALMTs). Front. Plant Sci. **3:** 263.

Eisenach, C., and De Angeli, A. (2017). Ion transport at the vacuole during stomatal movements. Plant Physiol. **174:** 520–530.

Fuglsang, A.T., Guo, Y., Cuin, T.A., Qiu, Q., Song, C., Kristiansen, K.A., Bych, K., Schulz, A., Shabala, S., Schumaker, K.S., Palmgren, M.G., and Zhu, J.K. (2007). Arabidopsis protein kinase PKS5 inhibits the plasma membrane H^+ -ATPase by preventing interaction with 14-3-3 protein. Plant Cell **19:** 1617–1634.

Gago, J., Daloso, D de M., Figueroa, C.M., Flexas, J., Fernie, A.R., and Nikoloski, Z. (2016). Relationships of leaf net photosynthesis, stomatal conductance, and mesophyll conductance to primary metabolism: A multispecies meta-analysis approach. Plant Physiol. **171:** 265–279.

Geiger, D., Becker, D., Vosloh, D., Gambale, F., Palme, K., Rehers, M., Anschuetz, U., Dreyer, I., Kudla, J., and Hedrich, R. (2009). Heteromeric AtKC1middle dotAKT1 channels in Arabidopsis roots facilitate growth under K+-limiting conditions. J. Biol. Chem. **284:** 21288–21295.

Gerhardt, R., and Heldt, H.W. (1984). Measurement of subcellular metabolite levels in leaves by fractionation of freeze-stopped material in nonaqueous media. Plant Physiol. **75:** 542–547.

Gleave, A.P. (1992). A versatile binary vector system with a T-DNA organisational structure conducive to efficient integration of cloned DNA into the plant genome. Plant Mol. Biol. **20:** 1203–1207.

Gobert, A., Isayenkov, S., Voelker, C., Czempinski, K., and Maathuis, F.J.M. (2007). The two-pore channel TPK1 gene encodes the vacuolar K^+ conductance and plays a role in K^+ homeostasis. Proc. Natl. Acad. Sci. USA **104:** 10726–10731.

Hafke, J.B., Hafke, Y., Smith, J.A.C., Lüttge, U., and Thiel, G. (2003). Vacuolar malate uptake is mediated by an anion-selective inward rectifier. Plant J. **35:** 116–128.

Heazlewood, J.L., Durek, P., Hummel, J., Selbig, J., Weckwerth, W., Walther, D., and Schulze, W.X. (2008). PhosPhAt: a database of phosphorylation sites in *Arabidopsis thaliana* and a plant-specific phosphorylation site predictor. Nucleic Acids Res. **36:** D1015–D1021.

Hettenhausen, C., Baldwin, I.T., and Wu, J. (2012). Silencing MPK4 in *Nicotiana attenuata* enhances photosynthesis and seed production but compromises abscisic acid-induced stomatal closure and guard cell-mediated resistance to *Pseudomonas syringae* pv tomato DC3000. Plant Physiol. **158:** 759–776.

Hille, B. (2001). Ion Channels of Excitable Membranes, 3rd ed. (Sunderland, MA: Sinauer Associates).

Hills, A., Chen, Z.-H., Amtmann, A., Blatt, M.R., and Lew, V.L. (2012). OnGuard, a computational platform for quantitative kinetic modeling of guard cell physiology. Plant Physiol. **159:** 1026–1042.

Hõrak, H., et al. (2016). A dominant mutation in the HT1 kinase uncovers roles of MAP kinases and GHR1 in CO_2-induced stomatal closure. Plant Cell **28:** 2493–2509.

Hosy, E., et al. (2003). The Arabidopsis outward K^+ channel GORK is involved in regulation of stomatal movements and plant transpiration. Proc. Natl. Acad. Sci. USA **100:** 5549–5554.

Imes, D., Mumm, P., Böhm, J., Al-Rasheid, K.A.S., Marten, I., Geiger, D., and Hedrich, R. (2013). Open stomata 1 (OST1) kinase controls R-type anion channel QUAC1 in Arabidopsis guard cells. Plant J. **74:** 372–382.

Ito, T., Motohashi, R., Kuromori, T., Mizukado, S., Sakurai, T., Kanahara, H., Seki, M., and Shinozaki, K. (2002). A new resource of locally transposed Dissociation elements for screening gene-knockout lines in silico on the Arabidopsis genome. Plant Physiol. **129:** 1695–1699.

Jakobson, L., et al. (2016). Natural variation in Arabidopsis Cvi-0 accession reveals an important role of MPK12 in guard cell CO_2 signaling. PLoS Biol. **14:** e2000322.

Jammes, F., et al. (2009). MAP kinases MPK9 and MPK12 are preferentially expressed in guard cells and positively regulate ROS-mediated ABA signaling. Proc. Natl. Acad. Sci. USA **106:** 20520–20525.

Johansson, I., Wulfetange, K., Porée, F., Michard, E., Gajdanowicz, P., Lacombe, B., Sentenac, H., Thibaud, J.-B., Mueller-Roeber, B., Blatt, M.R., and Dreyer, I. (2006). External K^+ modulates the activity of the Arabidopsis potassium channel SKOR via an unusual mechanism. Plant J. **46:** 269–281.

Jossier, M., Kroniewicz, L., Dalmas, F., Le Thiec, D., Ephritikhine, G., Thomine, S., Barbier-Brygoo, H., Vavasseur, A., Filleur, S., and Leonhardt, N. (2010). The Arabidopsis vacuolar anion transporter, AtCLCc, is involved in the regulation of stomatal movements and contributes to salt tolerance. Plant J. **64:** 563–576.

Kollist, H., Nuhkat, M., and Roelfsema, M.R.G. (2014). Closing gaps: linking elements that control stomatal movement. New Phytol. **203:** 44–62.

Kovermann, P., Meyer, S., Hörtensteiner, S., Picco, C., Scholz-Starke, J., Ravera, S., Lee, Y., and Martinoia, E. (2007). The Arabidopsis vacuolar malate channel is a member of the ALMT family. Plant J. **52:** 1169–1180.

Lee, M., Choi, Y., Burla, B., Kim, Y.-Y., Jeon, B., Maeshima, M., Yoo, J.-Y., Martinoia, E., and Lee, Y. (2008). The ABC transporter AtABCB14 is a malate importer and modulates stomatal response to CO_2. Nat. Cell Biol. **10:** 1217–1223.

Lee, Y., Kim, Y.J., Kim, M.-H., and Kwak, J.M. (2016). MAPK cascades in guard cell signal transduction. Front. Plant Sci. **7:** 80.

Leissing, F., Nomoto, M., Bocola, M., Schwaneberg, U., Tada, Y., Conrath, U., and Beckers, G.J.M. (2016). Substrate thiophosphorylation by Arabidopsis mitogen-activated protein kinases. BMC Plant Biol. **16:** 48.

Leung, J., Orfanidi, S., Chefdor, F., Mészaros, T., Bolte, S., Mizoguchi, T., Shinozaki, K., Giraudat, J., and Bögre, L. (2006). Antagonistic interaction between MAP kinase and protein phosphatase 2C in stress recovery. Plant Sci. **171:** 596–606.

Lovy-Wheeler, A., Kunkel, J.G., Allwood, E.G., Hussey, P.J., and Hepler, P.K. (2006). Oscillatory increases in alkalinity anticipate growth and may regulate actin dynamics in pollen tubes of lily. Plant Cell **18:** 2182–2193.

MacRobbie, E.A. (2000). ABA activates multiple $Ca^{(2+)}$ fluxes in stomatal guard cells, triggering vacuolar $K^{(+)}(Rb^{(+)})$ release. Proc. Natl. Acad. Sci. USA **97:** 12361–12368.

MacRobbie, E.A.C. (1995a). ABA-induced ion efflux in stomatal guard cells: multiple actions of ABA inside and outside the cell. Plant J. **7:** 565–576.

MacRobbie, E.A.C. (1995b). Effects of ABA on $^{86}Rb^{+}$ fluxes at plasmalemma and tonoplast of stomatal guard cells. Plant J. **7:** 835–843.

MacRobbie, E.A.C. (2006). Osmotic effects on vacuolar ion release in guard cells. Proc. Natl. Acad. Sci. USA **103:** 1135–1140.

MacRobbie, E.A.C., and Lettau, J. (1980). Ion content and aperture in "isolated" guard cells of *Commelina communis* L. J. Membr. Biol. **53:** 199–205.

Martinoia, E., and Rentsch, D. (1994). Malate compartmentation-responses to a complex metabolism. Annu. Rev. Plant Physiol. Plant Mol. Biol. **45:** 447–467.

Medeiros, D.B., Martins, S.C.V., Cavalcanti, J.H.F., Daloso, D.M., Martinoia, E., Nunes-Nesi, A., DaMatta, F.M., Fernie, A.R., and Araújo, W.L. (2016). Enhanced photosynthesis and growth in atquac1 knockout mutants are due to altered organic acid accumulation and an increase in both stomatal and mesophyll conductance. Plant Physiol. **170:** 86–101.

Meyer, S., Mumm, P., Imes, D., Endler, A., Weder, B., Al-Rasheid, K.A., Geiger, D., Marten, I., Martinoia, E., and Hedrich, R. (2010). AtALMT12 represents an R-type anion channel required for stomatal movement in Arabidopsis guard cells. Plant J. **63:** 1054–1062.

Meyer, S., Scholz-Starke, J., De Angeli, A., Kovermann, P., Burla, B., Gambale, F., and Martinoia, E. (2011). Malate transport by the vacuolar AtALMT6 channel in guard cells is subject to multiple regulation. Plant J. **67:** 247–257.

Michard, E., Simon, A.A., Tavares, B., Wudick, M.M., and Feijó, J.A. (2017). Signaling with ions: the keystone for apical cell growth and morphogenesis in pollen tubes. Plant Physiol. **173:** 91–111.

Mine, A., Berens, M.L., Nobori, T., Anver, S., Fukumoto, K., Winkelmüller, T.M., Takeda, A., Becker, D., and Tsuda, K. (2017). Pathogen exploitation of an abscisic acid- and jasmonate-inducible MAPK phosphatase and its interception by *Arabidopsis* immunity. Proc. Natl. Acad. Sci. USA **114:** 7456–7461.

Monda, K., Araki, H., Kuhara, S., Ishigaki, G., Akashi, R., Negi, J., Kojima, M., Sakakibara, H., Takahashi, S., Hashimoto-Sugimoto, M., Goto, N., and Iba, K. (2016). Enhanced stomatal conductance by a spontaneous Arabidopsis tetraploid, Me-0, results from increased stomatal size and greater stomatal aperture. Plant Physiol. **170:** 1435–1444.

Monda, K., Negi, J., Iio, A., Kusumi, K., Kojima, M., Hashimoto, M., Sakakibara, H., and Iba, K. (2011). Environmental regulation of stomatal response in the Arabidopsis Cvi-0 ecotype. Planta **234:** 555–563.

Montillet, J.-L., et al. (2013). An abscisic acid-independent oxylipin pathway controls stomatal closure and immune defense in Arabidopsis. PLoS Biol. **11:** e1001513.

Mumm, P., Imes, D., Martinoia, E., Al-Rasheid, K.A.S., Geiger, D., Marten, I., and Hedrich, R. (2013). C-terminus-mediated voltage gating of Arabidopsis guard cell anion channel QUAC1. Mol. Plant **6:** 1550–1563.

Munemasa, S., Hauser, F., Park, J., Waadt, R., Brandt, B., and Schroeder, J.I. (2015). Mechanisms of abscisic acid-mediated control of stomatal aperture. Curr. Opin. Plant Biol. **28:** 154–162.

Obulareddy, N., Panchal, S., and Melotto, M. (2013). Guard cell purification and RNA isolation suitable for high-throughput transcriptional analysis of cell-type responses to biotic stresses. Mol. Plant Microbe Interact. **26:** 844–849.

Pfaffl, M.W. (2001). A new mathematical model for relative quantification in real-time RT-PCR. Nucleic Acids Res. **29:** e45.

Roelfsema, M.R.G., and Hedrich, R. (2005). In the light of stomatal opening: new insights into 'the Watergate'. New Phytol. **167:** 665–691.

Roelfsema, M.R.G., and Hedrich, R. (2010). Making sense out of $Ca^{(2+)}$ signals: their role in regulating stomatal movements. Plant Cell Environ. **33:** 305–321.

Sasaki, T., Mori, I.C., Furuichi, T., Munemasa, S., Toyooka, K., Matsuoka, K., Murata, Y., and Yamamoto, Y. (2010). Closing plant stomata requires a homolog of an aluminum-activated malate transporter. Plant Cell Physiol. **51:** 354–365.

Sato, A., Sato, Y., Fukao, Y., Fujiwara, M., Umezawa, T., Shinozaki, K., Hibi, T., Taniguchi, M., Miyake, H., Goto, D.B., and Uozumi, N. (2009). Threonine at position 306 of the KAT1 potassium channel is essential for channel activity and is a target site for ABA-activated SnRK2/OST1/SnRK2.6 protein kinase. Biochem. J. **424:** 439–448.

Sparkes, I.A., Runions, J., Kearns, A., and Hawes, C. (2006). Rapid, transient expression of fluorescent fusion proteins in tobacco plants and generation of stably transformed plants. Nat. Protoc. **1:** 2019–2025.

Su, J., Zhang, M., Zhang, L., Sun, T., Liu, Y., Lukowitz, W., Xu, J., and Zhang, S. (2017). Regulation of stomatal immunity by interdependent functions of a pathogen-responsive MPK3/MPK6 cascade and abscisic acid. Plant Cell **29:** 526–542.

Takahashi, S., et al. (2015). Natural variation in stomatal responses to environmental changes among *Arabidopsis thaliana* ecotypes. PLoS One **10:** e0117449.

Van Kirk, C.A., and Raschke, K. (1978). Presence of chloride reduces malate production in epidermis during stomatal opening. Plant Physiol. **61:** 361–364.

Wege, S., De Angeli, A., Droillard, M.-J., Kroniewicz, L., Merlot, S., Cornu, D., Gambale, F., Martinoia, E., Barbier-Brygoo, H., Thomine, S., Leonhardt, N., and Filleur, S. (2014). Phosphorylation of the vacuolar anion exchanger AtCLCa is required for the stomatal response to abscisic acid. Sci. Signal. **7:** ra65.

Wingenter, K., Trentmann, O., Winschuh, I., Hörmiller, I.I., Heyer, A.G., Reinders, J., Schulz, A., Geiger, D., Hedrich, R., and Neuhaus, H.E. (2011). A member of the mitogen-activated protein 3-kinase family is involved in the regulation of plant vacuolar glucose uptake. Plant J. **68:** 890–900.

Xing, Y., Jia, W., and Zhang, J. (2008). AtMKK1 mediates ABA-induced CAT1 expression and H_2O_2 production via AtMPK6-coupled signaling in Arabidopsis. Plant J. **54:** 440–451.

Zhang, J., Baetz, U., Krügel, U., Martinoia, E., and De Angeli, A. (2013). Identification of a probable pore-forming domain in the multimeric vacuolar anion channel AtALMT9. Plant Physiol. **163:** 830–843.

Zhang, J., Martinoia, E., and De Angeli, A. (2014). Cytosolic nucleotides block and regulate the Arabidopsis vacuolar anion channel AtALMT9. J. Biol. Chem. **289:** 25581–25589.

Zhang, X., Henriques, R., Lin, S.S., Niu, Q.W., and Chua, N.H. (2006). Agrobacterium-mediated transformation of Arabidopsis thaliana using the floral dip method. Nat. Protoc. **1:** 641–646.

Zheng, J. (2013). Domain-domain interactions in ion channels. J. Gen. Physiol. **142:** 347–350.